

Spatial Super Resolution Based Image Reconstruction using IBP and Evolutionary Method



S Monalisa

Roll No.: 211EE1143

Department of Electrical Engineering
National Institute of Technology, Rourkela
Rourkela-769008, Odisha, INDIA

June 2013

Spatial Super Resolution Based Image Reconstruction using IBP and Evolutionary Method

A thesis submitted in partial fulfillment of the
requirements for the degree of

Master of Technology

in

Electronics Systems & Communication

by

S Monalisa

(Roll-211EE1143)

Under the Guidance of

Dr. (Prof.) Dipti Patra



Department of Electrical Engineering

National Institute of Technology, Rourkela

Rourkela-769008, Odisha, INDIA

2011-2013

Department of Electrical Engineering

National Institute of Technology, Rourkela

C E R T I F I C A T E

*This is to certify that the thesis entitled “Spatial Super Resolution Based Image Reconstruction using IBP and Evolutionary Method” by Ms. S Monalisa, submitted to the National Institute of Technology, Rourkela (Deemed University) for the award of Master of Technology in **Electrical Engineering** with the specialization of “**Electronic Systems and Communication**”, is a record of bonafide research work carried out by her in the **Department of Electrical Engineering**, under my supervision. I believe that this thesis fulfills part of the requirements for the award of degree of Master of Technology. The results embodied in the thesis have not been submitted for the award of any other degree elsewhere.*

Dr. (Prof.) Dipti Patra

Dept. of Electrical Engineering

National Institute of Technology

Rourkela, Odisha, 769008

Place: N.I.T., Rourkela

Date:

INDIA

Acknowledgement

I would like to express my deepest gratitude to my advisor Dr.(Prof.) Dipti Patra for her guidance and support. Her sharp knowledge, creativity and excellent analytical skills have always been a constant source of motivation for me. The perfection that she brings to each and every piece of work that she does always inspired me to do things right at first time. She is a great person and one of the best mentors, I always be thankful to her.

I would like to sincerely thank my Professors; Prof. P. K. Sahu, Prof. Sushmita Das, Prof. K. R. Shubhashini and Prof. Supratim Gupta for their caring guidance and valuable teachings.

My sincere thanks must also go to the members of my thesis advisory: Ms. Smita Pradhan, Ms. Prajna Dash and Mr. Yogananda Patnaik. They generously gave their time to offer me valuable comments toward improving my work.

I am very much grateful to Sushant Sawant for his generous help in particular issues related to simulations. I cannot forget friends who went through hard times together, cheered me on, and celebrated each accomplishment. Thanks for the unforgettable time: Maithri, Medhavi, Vipin and many others.

These acknowledgments would not be complete without thanking my family for their constant support and care. I would like to express my gratitude to my parents for their unfailing emotional support.

S Monalisa

NIT Rourkela, 2013

ABSTRACT

Spatial image resolution explains about the pixel spacing in a digital image. As a result more the number of pixels more detailed visibility of information contained in the image. Increasing the sensor elements per unit area in camera is the solution to high resolution images but at higher cost, since increase in camera resolution increases the cost of the camera. Another limitation to this is hardware part of the camera *i.e.* we cannot minimize the sensor element size beyond the optimum limit. Therefore an imaging system with inadequate sensor array will generate low resolution image which causes pixelization effect in them.

To resolve the above problem software level techniques are adopted. Interpolation of a 2D signal improves the size of the image with additional row and column values. As interpolation averages pixel intensity with neighboring pixels and assigns the result to new pixels in HR image, the HR image loses edge information because of blurring or aliasing. To improve image resolution while avoiding aliasing effect we are using Super Resolution Image Reconstruction technique. As the application of image reconstruction in Computer Tomography (CT) is capturing multiple 2D images with known depth information can create 3D picture of an infected tissue, here we are using multiple number of low resolution images with subpixel shift that provide non-redundant information about the scene and generate a HR image with more high frequency details.

This reconstruction problem uses iterative back projection technique along with evolutionary techniques for optimization. In our image observation model, three lacunae of LR images have been considered, *i.e.* relative motion between scene and camera, sensor blur and down-sampling during image acquisition. In the inverse model we use the above calculated parameters in back projection. Iteratively the reverse model is solved to find the HR image; this method is also called as gradient based method. As the gradient remains constant over here, the solution it provides may not be the best and hence the requirement of optimization technique. The nature inspired optimization algorithm used here is Cuckoo optimization algorithm with Lèvy flights.

Contents

Acknowledgment.....	i
Abstract.....	ii
List of Figures.....	v
List of Tables.....	vii
List of Acronyms.....	viii
1. Introduction.....	1
1.1 Introduction.....	1
1.2 Image reconstruction.....	1
1.3 Image resolution.....	2
1.4 Motivation.....	2
1.4.1 Interpolation and its limitations.....	2
1.4.2 Hardware limitations.....	3
1.4 Super resolution	4
1.5 Literature Review.....	6
1.6 Contributions of the thesis.....	7
1.7 Organization of thesis.....	7
2. Reconstruction of images using Spatial Super Resolution.....	8
2.1. Image observation model.....	8
2.2 Mathematical expression.....	11
2.2.1. Forward model.....	11
2.2.1.1. Geometrical Warp operator.....	12
2.2.1.2. Blur operator.....	15
2.2.1.3. Down-sampling operator.....	16
2.2.1.4. Data Model.....	18

2.2.2.	SR Inverse Model.....	20
2.3	Iterative Back Projection Technique.....	20
2.4	Optimization technique.....	22
2.4.1	Cuckoo Optimization Method.....	23
3.	Simulations and Result Analysis.....	26
3.1	Simulations.....	26
3.2	Simulations using synthetic data.....	27
3.3	Image quality Assessment.....	35
3.3.1	Mean Square Error.....	35
3.3.2	SSIM.....	35
3.3.3	Result Analysis.....	40
4.	Conclusion & Future Research	45
4.1	Conclusion.....	45
4.2	Future work directions.....	46
	Bibliography.....	47

List of Figures

1.1	<i>Two low resolution images with sub-pixel shift and non redundant visual information.....</i>	4
1.2	<i>Relationship between low resolution images and high resolution image.....</i>	5
1.3	<i>Drawn here to show importance of sub-pixel shift.....</i>	5
2.1	<i>Image observation model. Input to the model is a reference HR image which undergoes affine transformation, blur and down-sampling along with added noise gives multiple number of low resolution images. The output of each block is shown in corresponding camera man image.....</i>	9
2.2	<i>Forward and Inverse view of Image observation Model.....</i>	11
2.3	<i>Random egg laying in ELR, central red star is the initial habitat of the cuckoo with 5 eggs; pink stars are the eggs' new nest.....</i>	25
3.1	<i>Flow chart of conventional Cuckoo Optimization Algorithm LR Image, (b) HR image, where both of the images are shown in same scale.....</i>	27
3.2	<i>(a)color image captured by the SAMSUNG GT-S7562 camera, (b) after resizing the previous image to 512×512 resolution, (c-f) shows 4 low resolution images each with unique information, (g) bicubic interpolation of one of the LR image, (h) Super resolution solution using IBP method and (i) super resolved HR image from IBP and Cuckoo optimization algorithm.....</i>	28
3.3	<i>Image data for the “Baby” example. (a) Ground truth for the baby image. (b-e) Four of the low-resolution images generated as synthetic inputs for super-resolution technique. (f) HR image reconstructed using SR Iterative Back Projection method; (g) HR image reconstructed using SR IBP method along with Cuckoo Optimization Algorithm; (h) Bicubic interpolation.....</i>	30
3.3.1	<i>Image data for the “Baby” example. (a) Ground truth for the baby image. (b-d) Three of the low-resolution images generated as synthetic inputs for super-resolution technique. (e) a low-resolution image rotated anti-clockwise with a very small angle.</i>	

	(f) HR image reconstructed using SR Iterative Back Projection method; (g) HR image reconstructed using the SR IBP method along with Cuckoo Optimization Algorithm;(h)Bicubic Interpolation.....	31
3.4	Image data for the “Wheel” example (a) The ground truth wheel image. (b-j) Four of the low-resolution images generated as synthetic inputs for super-resolution technique. (k) HR image reconstructed using SR Iterative Back Projection method, (l). HR image reconstructed using SR IBP method along with Cuckoo Optimization Algorithm, (m) Bicubic interpolation.....	32
3.5	Image data for the “camera man” example (a) The ground truth camera man image. (b-q) Sixteen of the low-resolution images generated as synthetic inputs for super-resolution technique. (r) HR image reconstructed using SR Iterative Back Projection method. (s) HR image reconstructed using SR IBP method along with Cuckoo Optimization Algorithm. (t) Bicubic interpolation.....	33-34
3.6	shows the test images used here for assessment of quality of the super resolved image. (a) Tier, (b) Pout, (c) “Deer”, (d) “Baby”, (e) “Blocks”, (f) “Scale”, (g) “Kids”, (h) “Brain MRI”, (i) “Satellite”, (j) “Camera Man” image.....	38
3.7	Comparison with 9 number of LR images at input, (a) mean square error values for SR IBP generated HR image(shown in red line) and SR IBP+COA generated HR images(shown in blue line), (b) SSIM index for SR IBP generated HR image(shown in green line) and SR IBP+COA generated HR images(shown in red line).....	42
3.8	Comparison with 9 number of LR images at input, (a) mean square error values for SR IBP generated HR image(shown in red line) and SR IBP+COA generated HR images(shown in blue line), (b) SSIM index for SR IBP generated HR image(shown in green line) and SR IBP+COA generated HR images(shown in red line).....	43
3.9	Comparison with 16 number of LR images at input, (a) mean square error values for SR IBP generated HR image(shown in red line) and SR IBP+COA generated HR images(shown in blue line), (b) SSIM index for SR IBP generated HR image(shown in red line) and SR IBP+COA generated HR images(shown in blue line).....	44

List of Tables

3.1	<i>Table showing comparision of SR IBP and SR IBP + COA technique using MSE and SSIM index for image quality assessment, each done for 4, 9 and 16 LR images case.....</i>	39
------------	--	-----------

List of Acronyms

Algo.	Algorithm
CAT	Computer Aided Tomography
CCD	Charge Coupled Device
CMOS	Complementary Metal-Oxide Semiconductor
COA	Cuckoo Optimization Algorithm
GA	Genetic Algorithm
HR	High Resolution
IBP	Iterative Back Projection
IQA	Image Quality Assessment
LR	Low Resolution
MSE	Mean Square Error
PSF	Point Spread Function
PSO	Particle Swarm Optimization
SR	Super Resolution
SSIM	Structural SIMilarity index

Dedicated to my Beloved Parents

Chapter 1

Introduction

1.1 Introduction

Digital images are ubiquitously used now a days for various purposes. Digital image processing helps to extract pictorial details along with useful information from the given image of lower quality.

The basic functional units of image processing are; a. Image acquisition system such as a video camera, scanner or frame grabber, b. Processing and storage system such as a memory or a computer and c. Display module *e.g.* a monitor or printer. In applications like satellite imaging, medical imaging, microscopy, security systems, archeology study *etc.* it is always desirable to have images with detailed information. In other words higher resolution images are most preferred for their detailed information also, high resolution (HR) images provide better edge details, classification of regions along with a more pleasing view of the human eye. The resolution of an image is dependent on its sensor resolution, hence to acquire higher resolution one will need complex image acquisition devices which may be very costly and may not be affordable. However, digital image processing provides software level cost friendly techniques to construct higher resolution images.

1.2 Image Reconstruction

Image reconstruction is a mathematical process for creation of 2D or 3D images, providing meaningful information, from scattered or incomplete data. It applies mathematical techniques to generate readable and usable image or sharpen an image to make it useful. In computed Tomography (CT) it is used to generate a 3D image of the body from a series of individual camera images from X-Ray projections data acquired at many different angles around the patient [1]. In archeology, researchers need to investigate the findings without causing any damage to them. Reconstruction helps in constructing the useful data back projected from multiple numbers of 2D images which are having insufficient data as a single [2].

A computer can simulate & produce HR images from low resolution (LR) ones using reconstruction technique. The super resolution technique is one of the most important technique used in reconstruction of HR image.

1.3 Image resolution

Image Resolution is a very important term in image processing which simultaneously judges the quality of various image acquisitions and processing devices. Image Resolution, in simple words, can be defined as the smallest measurable detail in a visual presentation.

In digital image processing we have three different types of image resolution parameters, such as: spatial resolution, brightness resolution and temporal resolution. In this thesis, spatial resolution is considered, as it says about the spacing of pixels in an image and is measured in pixels per inch (ppi). The higher the spatial resolution of an image, greater the number of pixels in the image accordingly, smaller the size of individual pixels will be. This allows for more detail and subtle color transitions in an image. The spatial resolution of a display device is often expressed in terms of dots per inch (dpi) and it refers to the size of the individual spots created by the device [28].

1.4 Motivation

The requirement of zooming in images to view and analyze visual information with greater details increases in medical applications, satellite applications *etc.* the best image acquisition systems are of greater cost while images produced by these cameras still have distortions [5].

1.4.1 Interpolation and its Limitations

Interpolation is the simplest way to increase the size of the image. Basically, interpolation uses known data to estimate values at unknown locations. Suppose that an image of size $(680 * 680)$ pixels has to be enlarged 1.5 times to $(1024 * 1024)$. To visualize this zooming let's think of enlarging an image of $(680 * 680)$ pixel size to $(1024 * 1024)$, i.e. create a grid of size $(1024 * 1024)$ and shrink it so that it will fit to the original image of size $(680 * 680)$ thus changing the pixel spacing of $(1024 * 1024)$ grid. Now the intensity values in the grid will take from the original image and upon changing the pixel spacing of new images to earlier value we will get the zoomed image. Different techniques of interpolation are nearest neighbor interpolation, bicubic interpolation and bilinear interpolation [28].

According to the previous example the pixels of zooming image just take intensity information from original image pixel and its neighboring pixels, which causes blur effect. A new image is larger in size but provides aliased or blurred information of the LR image.

1.4.2 Hardware limitations

The important factors that limit the performance of the cameras in consumer devices are:

- Spatial frequency response of the camera.
- Optical system distortion like geometrical aberrations.
- Sub-sampling of different spectral components, mostly affecting the high frequency information.
- Photo-detector noise and quantization error causing aliasing.
- Hardware design limitations because of packaging and power consumption.

Hardware design of a camera system considers several important criteria such as; lens type, sensor type, pixel size, interconnections, control electronics, clocking system, power supply, dynamic range coverage, shuttering *etc.* The final image resolution is dependent on a combination of all of the above mentioned design components.

The most employed sensor technology in camera is a charge coupled device (CCD) technology and complementary metal oxide semiconductor (CMOS) technology. The employed sensor technology causes the main limitation to image resolution, both CMOS and CCD technology sense light through similar mechanism *i.e.*, by applying the photo-electric effect that occurs when photons interact with crystallized silicon to excite electrons from the valence band to the conduction band. In Figure 1.1 the circle inside each pixel area represents the actual photosensitive area.

Therefore, the more innate way to increase the spatial super resolution has been to reduce the pixel area. This made continuous decrease in pixel size from 10-20 microns to 2-3 microns which are currently available in the market. Nevertheless, since semiconductor capacitance is proportional to the semi - conductor area, it requires a trade-off between the pixel size and light sensitivity. Hence smaller pixels require bright sunlight or flash to obtain an acceptable SNR level, fabrication process cost and other fundamental optical limits which increase the cost of consumer cameras along with more power consumption [3].

Based on previously mentioned arguments it can be concluded that a mere increase in pixel count or decrease in pixel size will no longer be enough for spatial resolution enhancement, to follow the trend sophisticated signal processing tools will be needed.

1.5 Super Resolution

Super resolution is an image reconstruction problem which generates a high resolution image from a number of low resolution images, each differs in sub-pixel shift parameter, blur parameter etc. from one another. Each low resolution image that has new unique information for the high resolution image is useful for the super resolution technique.

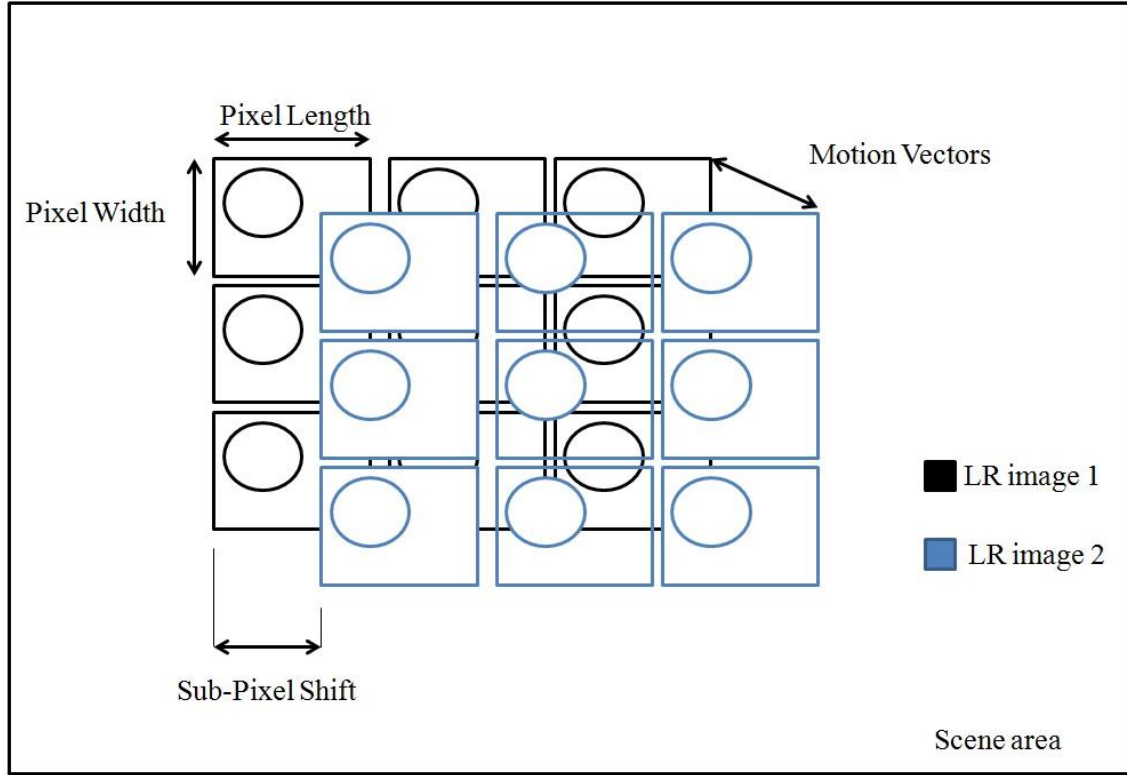


Figure 1.1: Two low resolution images with sub-pixel shift and non redundant visual information

It is a method of extrapolation *i.e.* the process of estimation, beyond the original observation interval. As figure 1.1 explains this; let a scene is being captured by a camera of (3×3) resolution. A unit of sensor as known as pixel has a fixed dimension. The circle inside each pixel shows the approximate photosensitive area of the pixel hence the light falling on the pixel other than the photosensitive area cannot be captured by LR frame1. Therefore the use of extrapolation enables taking information from another observation *i.e.* LR frame2 with sub-pixel shift of LR image 1. An important point to be considered is that only images with sub-pixel shift only can provide non-redundant information (motion vectors), to visualize it

the second column of pixel for LR image 2 are drawn transparent showing the un-overlapped photo sensitive area.

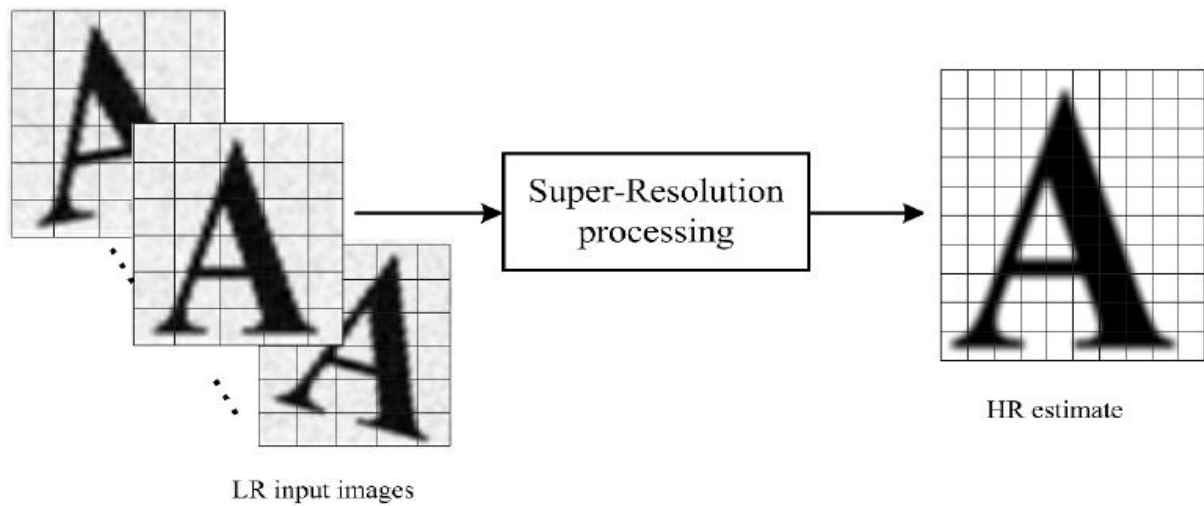


Figure 1.2: Relationship between low resolution images and high resolution image.

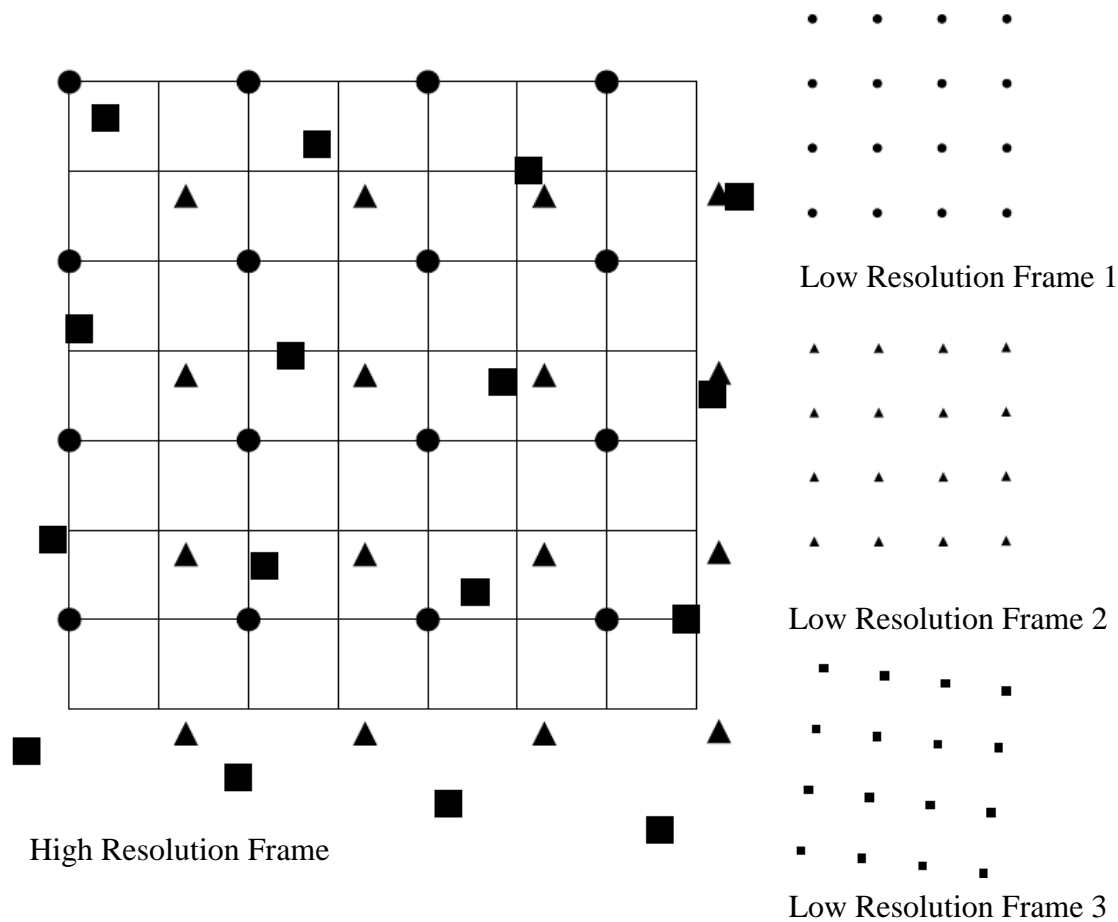


Figure 1.3: drawn here to show importance of sub-pixel shift.

It uses extrapolation for resolution enhancement in the reconstructed image. The high frequency components for HR images are extrapolated from multiple numbers of LR images. It applies 2D-signal processing techniques to eliminate hardware limitations.

The set of low resolution images are first mutually aligned on a common high resolution lattice. This is generally referred to as image registration. The aligned pixel values (usually resulting in a non-uniform sampling) are then interpolated over the reference high resolution lattice to obtain a fused high resolution image as shown in figure 1.2. A subsequent de-blurring of the fused image results in a higher resolution image provided that a sufficient number of low resolution images are available and that the image alignment is carried out to sub-pixel accuracy. While these subtasks have been separately identified for conceptual clarity, they are often performed in a joint fashion [4].

Figure 1.3 shows mapping of 4 number of (4×4) LR images onto a (8×8) HR grid. Where each of the 4 LR image with different sub-pixels shift *i.e.* each with unique information of the object are projected onto HR grid.

1.6 Literature Review

The basic of super resolution theory was laid by Papoulis *et. al.* in 1977 [6] is for 1D signal. It explained how a continuous band limited signal gets reconstructed from its convolution samples. This simple idea was upgraded to 2D signals or images by Huang & Tsai *et. al* in 1984 [7], with the concept of aliasing effect and considering images are noise free and band limited. This work was then applied to noisy images by Kim *et. al* least square minimization method in 1990 [8].

In 1992 Ur and Gross *et. al.* considered sub-pixel shift in low resolution images for the first time, with known 2D translation information [9]. They used de-blurring technique also had a limitation on no. of low resolution images used for this purpose.

Based on above approach Irani & Peleg *et. al.* suggested a technique on super resolution with image registration in 1991 [11]. The proposed approach is similar to Iterative back projection (IBP) used in Computer Aided Tomography (CAT). Keren *et. al.* included translation and rotation information for image registration to the previous work.

The algorithm starts with an initial guess, and iteratively simulates the imaging process, re-projecting the error back to the super resolution image. Hence the iterative back projection based reconstruction is an inversion problem using the gradient descent method to find a solution. Since inverse problems are ill-posed problems, they need regularization or optimization of the solution [10].

In 2001 Milanfar *et. al.* solved the above problem along with Tikhonov regularization [15], but the regularization methods have to introduce additional information called as regularization matrix, in order to prevent over fitting and solve the ill posed problem.

The iterative back projection technique is an ill-conditioned linear algebraic problem which resembles an undetermined system with never unique solution, hence can be solved using multi-objective optimization algorithms [24] [25]. X. S. Yang and S. Deb *et. al.* in 2009 explained one of the meta-heuristic method with Lèvy Flights to solve the inverse problem using evolutionary approaches.

1.7 Contribution of the thesis

The significant contribution of this thesis is providing multi-modal optimization technique to ill-posed inverse problem. Generation of HR image from LR samples using back projection is an inverse problem, solving it with iterative gradient based methods provides local solutions. Cuckoo optimization algorithm, one of the meta-heuristic methods, in global optimization techniques applies to the conventional IBP method.

1.8 Organization of thesis

The thesis is organized as follows:

- Chapter 1 gives an introduction to super resolution reconstruction problem.
- Chapter 2 describes the image observation model, problem formulation and the optimization technique used.
- Chapter 3 discusses simulation and result analysis.
- Chapter 4 concludes the thesis.

Chapter 2

Reconstruction of images using Spatial Super Resolution

2.1. Image Observation Model

The finite aperture size in the camera causes optical blur in the images which is modeled mathematically using point spread function (PSF). The limited sensor density causes an aliasing effect in images leads to lower spatial resolution of images. The confined sensor size of the camera is the reason to sensor blur which means the image pixel are generated by integration over the sensor area rather impulse sampling. The finite aperture time causes motion blur in images or videos also. The above discussed degradations are designed in different super resolution techniques either fully or partially.

Figure 2.1 shows a typical image observation model showing the HR image with LR images, as brought in the literature [4]. The input to the image observation model is continuous natural scenes. The images are well approximated as band-limited 2D signals. Atmospheric turbulence may cause contamination to these images before reaching the imaging system. High resolution digital images can be constructed by sampling the continuous 2D signal beyond the Nyquist rate. In the super resolution technique we require,

- a. Relative motion between the camera and scene. The inputs to the camera are multiple frames of the scene, connected by possibly sub-pixel shifts.
- b. Inside the camera, the affine-motion related high-resolution frames will induce optical blur and motion blur.
- c. The above blurred images are now down-sampled at the image sensors (e.g., CCD detectors or CMOS) into pixels, by an integral of the image falling into each sensor area.
- d. These down-sampled images get an additional noise by sensor noise and color filtering noise.

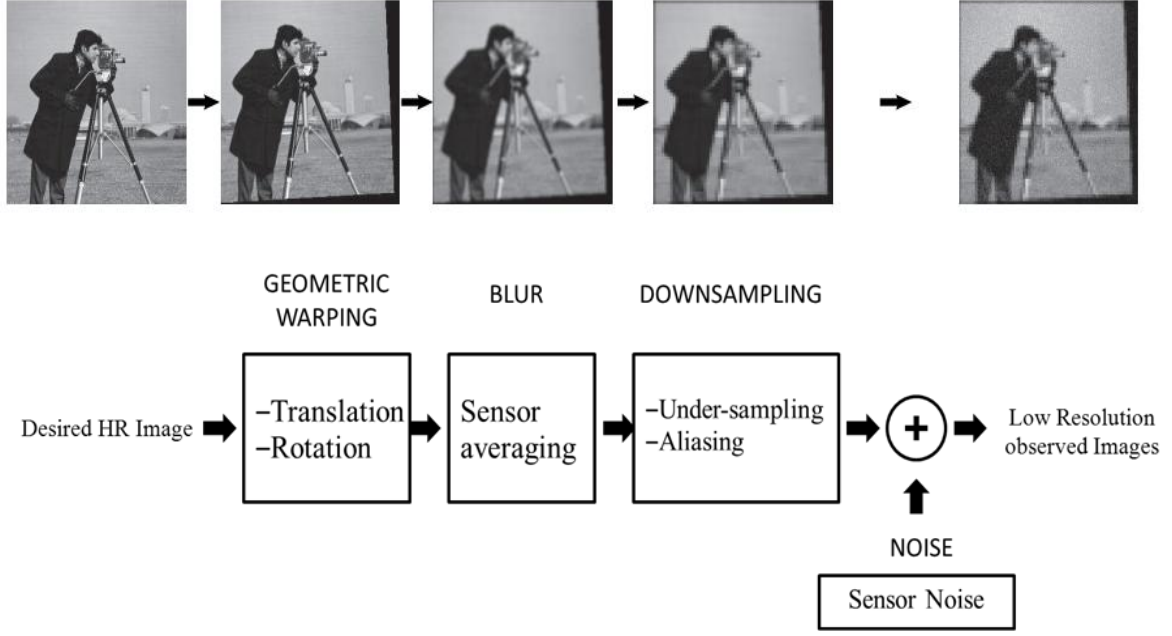


Figure 2.1: *image observation model. Input to the model is a reference HR image which undergoes affine-transformation, blur and down-sampling along with added noise gives a multiple number of low resolution images. The output of each block is shown in the corresponding camera man image.*

Finally, the frames captured by the low-resolution imaging system are blurred, decimated, and noisy versions of the underlying true scene.

The classic model of SR in the spatial domain assumes that a sequence of N low resolution images represents different snapshots of the same scene.

The real scene is to be predicted is represented by a single high resolution reference image X of size $(P \times P)$ each low resolution frame y_1, y_2, \dots, y_N is a noisy down-sampled version of the reference image i.e. subjected to the above mentioned image acquisition conditions as optical, sensor & atmospheric blur, motion effect and affine-translation.

The size of each low resolution frame is $(M \times M)$ & $M < P$. Hence the observation model conveniently can be represented in matrix notation

$$\begin{bmatrix} y_1 \\ y_2 \\ y_3 \\ \vdots \\ y_N \end{bmatrix} = \begin{bmatrix} D_1 \times B_1 \times W_1 \\ D_2 \times B_2 \times W_2 \\ D_3 \times B_3 \times W_3 \\ \vdots \\ D_N \times B_N \times W_N \end{bmatrix} \times X + \begin{bmatrix} e_1 \\ e_2 \\ e_3 \\ \vdots \\ e_N \end{bmatrix} = \begin{bmatrix} A_1 \\ A_2 \\ A_3 \\ \vdots \\ A_N \end{bmatrix} \times X + \begin{bmatrix} e_1 \\ e_2 \\ e_3 \\ \vdots \\ e_N \end{bmatrix} \quad (2.1)$$

Where D: Down-sampling matrix ($M^2 \times P^2$)

B: Blur matrix ($P^2 \times P^2$)

W: Geometric warp matrix ($P^2 \times P^2$)

By grouping and rewriting the equation no. 1 the model is given as

$$y = Ax + e \quad (2.2)$$

$$A_k = [D_k \times B_k \times W_k] \quad \text{for } k = 1, 2, \dots, N \quad (2.3)$$

Matrix A: linear operator ($M^2 \times P^2$)

LR frames: ($M^2 \times 1$)

Additive Gaussian noise: ($M^2 \times 1$)

The images are represented in equation 2.1 as vectors, shown by italicizing and are ordered column wise lexicographically.

Super resolution is a computationally very intensive process; hence the approach is to start with an initial-guess and successfully obtain more refined estimates. For example, Elad and Feuer *et. al.* used different approximations to the Kalman filter and evaluated their performance and considered recursive least squares (RLS), least mean squares (LMS), and steepest descent (SD) in particular [16]. Irani and Peleg *et. al.* defined a straightforward iterative scheme including both image registration and restoration, which uses a back-projection kernel [11].

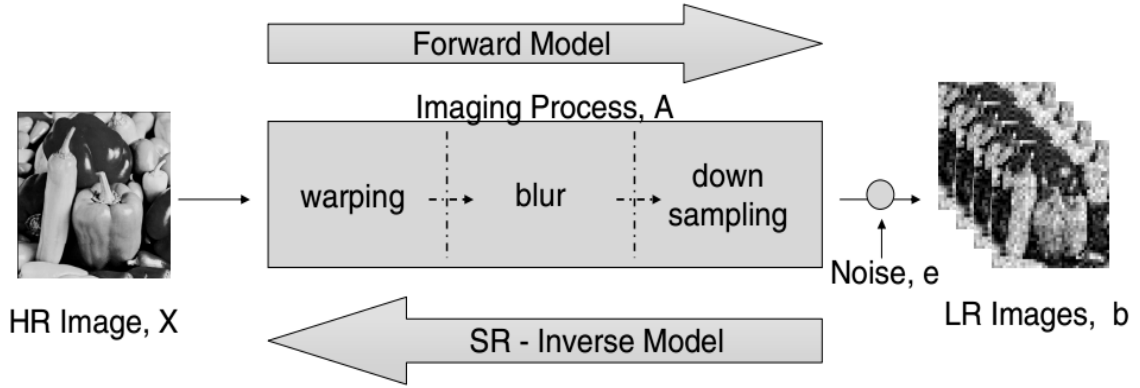


Figure 2.2: *Forward and Inverse view of Image observation Model.*

2.2. Mathematical Expression

A detailed study of the image acquisition system, from scene capture to formation of digital image, is required in order to apply a super resolution algorithm. In this section, we develop a mathematical model that converts an image that could be obtained with a high resolution camera to low resolution images that are typically captured by a low resolution camera. We then reconstruct the HR image by reversing the process. Our concept is matrix based. The forward model is perceived as matrix multiplication through construction of required operators, and the inverse model as a pseudo-inverse of a matrix *i.e.* calculated in the forward model.

2.2.1. Forward model

Let X be a HR grayscale image of size $P_x \times P_y$. Suppose that this image translationally and rotationally displaced, blurred and down-sampled, in that order. To capture N number of images, this process is repeated N times. Probably the displacements may differ each time, but the down-sampling factors and the blur parameter remain the same, which is generally true for real-world image acquisition system. Let W_1, W_2, \dots, W_N denote the sequence of affine-shifts and D the down-sampling factor, which may be different in the vertical and horizontal directions, *i.e.* there is D_x & D_y . Thus, we obtain N number of shifted, blurred, decimated versions y_1, y_2, \dots, y_N of the original image; these are called as observed images. Above Fig. 2.2 demonstrates this process with a fine image.

The “Original” or “Reference” image may not exist in real data. In that case, it viewed as an image that could be captured with a very high-quality camera which has a (D_x, D_y) times better resolution and does not have blur or it can be said that its point spread function (PSF) is a delta function.

To be able to represent above mentioned operations on the image as matrix multiplications, it's a requirement to convert the image (2D) matrix into a vector (1D form). Then we can design matrices which operate on each pixel of the image independently. For this purpose, we assign the 2 operators:

- **vec**; represents the lexicographic ordering of a matrix, forming a vector of vertical concatenation of matrix columns.
- **mat**; the inverse operator, which converts a vector into a matrix.

The dimensions of the matrix are not specified here explicitly to simplify the notation, but are assumed to be known.

Let $x = \text{vec}(X)$ and $y = \text{vec}(Y)$, $i = 1, \dots, N$ be the vectored versions of the reference image and the observed images, respectively. We can represent the successive transformations of x , warping, blurring, and down-sampling, separately from each other.

2.2.1.1. Geometrical warp Operator

A geometrical warp also called as a translational shift operator moves all rows or all columns of a matrix up or down by one. The row shift operator is denoted by W_x and the columns shift by W_y . Consider a sample matrix,

$$M_{ex} = \begin{bmatrix} 1 & 4 & 7 \\ 2 & 5 & 8 \\ 3 & 6 & 9 \end{bmatrix}$$

After a row shift in the upward direction, this matrix becomes

$$\text{mat}(W_x \text{vec}(M_{ex})) = \begin{bmatrix} 2 & 5 & 8 \\ 3 & 6 & 9 \\ 0 & 0 & 0 \end{bmatrix}$$

Note that the last row of the matrix was substituted by zeros. In fact, this depends on the boundary conditions. In this case, we assume that the matrix M_{ex} is zero padded around the boundaries, where zero represents black color, which corresponds to an image on a black

color background. Other boundary conditions are possible, for example the Dirichlet boundary, when there is no change along the boundaries, i.e. the image's derivative on the boundary is zero. Column shift operation is defined analogously to the row shift operation.

Most of the operators of interest have block diagonal form: only non-zero elements are contained along the main diagonal making sub-matrices. The notation $\text{diag}(A, B, C, \dots)$ is used to represent the block diagram concatenation of matrices A, B, C, \dots . Furthermore, most of the operators are composed of the same block repeated multiple times. Let $\text{diag}(\text{rep}(B, n))$ mean that the matrix B is diagonally concatenated with itself n times. Then the row shift can be expressed as a matrix whose diagonal blocks consist of the same sub-matrix B :

$$B = \begin{bmatrix} 0_{(n_x-1) \times 1} & I_{n_x-1} \\ 0_{1 \times 1} & 0_{1 \times (n_x-1)} \end{bmatrix}$$

The shift operators have the form:

$$W_x(1) = \text{diag}(\text{rep}(B, n_y))$$

$$W_y(1) = \begin{bmatrix} 0_{n_x(n_y-1) \times n_x} & I_{n_x(n_y-1)} \\ 0_{n_x \times n_x} & 0_{n_x \times n_x(n_y-1)} \end{bmatrix}$$

Here and thereafter, I_n denotes an identity matrix of size n ; $0_{n_x \times n_y}$ denotes a zero matrix of size $n_x \times n_y$. The total size of the zoom operator is $n_x n_y \times n_x n_y$. The notation $W_x(1), W_y(1)$ indicates that the shift is by one row or one column, to differentiate it from the multiple pixel shift, which is going to be described later.

Let us consider a 3×2 matrix M . Its corresponding row shift operator is:

$$W_x(1) = \begin{bmatrix} 0 & 1 & 0 & 0 & 0 & 0 \\ 0 & 0 & 1 & 0 & 0 & 0 \\ 0 & 0 & 0 & 0 & 0 & 0 \\ 0 & 0 & 0 & 0 & 1 & 0 \\ 0 & 0 & 0 & 0 & 0 & 1 \\ 0 & 0 & 0 & 0 & 0 & 0 \end{bmatrix}$$

It is apparent that this translation operator comprise diagonal concatenation of a matrix B with itself where,

$$B = \begin{bmatrix} 0 & 1 & 0 \\ 0 & 0 & 1 \\ 0 & 0 & 0 \end{bmatrix}$$

For the column shift operator,

$$W_y(1) = \begin{bmatrix} 0 & 0 & 0 & 1 & 0 & 0 \\ 0 & 0 & 0 & 0 & 1 & 0 \\ 0 & 0 & 0 & 0 & 0 & 1 \\ 0 & 0 & 0 & 0 & 0 & 0 \\ 0 & 0 & 0 & 0 & 0 & 0 \\ 0 & 0 & 0 & 0 & 0 & 0 \end{bmatrix}$$

The operators just have to be transposed for a translation operation in the opposite direction (the shifts above were considered to be down and to the right). So, $W_x(-1) = W_x^T(1)$, $W_y(-1) = W_y^T(1)$.

In multi-pixel shift case translation operators can be achieved by raising the one pixel shift operator to the power equal to the size of the chosen shift. [20] Thus, the notation $W_x(i), W_y(i)$ denotes the shift operator corresponding to the displacement (d_{ix}, d_{iy}) between the frames i and $i-1$, where $W_i = W_x(d_{ix})W_y(d_{iy})$. As an example, consider the shift operators for the same matrix as before, but now for a 2-pixel shift:

$$W_x(2) = W_x^2(1) = \begin{bmatrix} 0 & 0 & 1 & 0 & 0 & 0 \\ 0 & 0 & 0 & 0 & 0 & 0 \\ 0 & 0 & 0 & 0 & 0 & 0 \\ 0 & 0 & 0 & 0 & 0 & 1 \\ 0 & 0 & 0 & 0 & 0 & 0 \\ 0 & 0 & 0 & 0 & 0 & 0 \end{bmatrix}$$

An all zero matrix would be used for the column shift operator in this case, since the matrix it is applied to only have two elements. Though the construction of multiple shift operators from single shift ones is clear. It should be noticed that simply raising a matrix to a power may not work for any of the sophisticated boundary conditions, just like the reflexive boundary condition. In such a case, the shift operators required to be modified for every shift independently, depending on what the elements outside the boundary are assumed to be [20].

Rotational operator is one of the affine-transforms, which works just like translational operator. Rotation with the angle θ around the axis perpendicular to the image, has the matrix representation as

$$R = \begin{bmatrix} \cos \theta & -\sin \theta & 0 \\ \sin \theta & \cos \theta & 0 \\ 0 & 0 & 1 \end{bmatrix}$$

A multi-dimensional spatial structure is formed for affine transformation purpose the matrix R is used to calculate scaling parameter. According to this parameter the image under observation is rotated and correlation between the observation image and image under test is calculated, the scale parameter with minimum correlation gives image rotation information which is used during back projection.

2.2.1.2. Blur Operator

Blur is a natural property of every image acquisition device caused by the inadequacy of their optical systems. Other factors that can also cause blurring are such as motion generating motion blur and the presence of air introducing atmospheric blur, which we do not consider here. Here Lens blur or called as sensor blur is considered which can be modeled by the convolution of the image with a mask, represented by a matrix, corresponding to the optical system's point spread function (PSF). Blurring is a simple neighborhood averaging process. 2D Gaussian distribution is commonly used for blur model. This assimilates to the image being convolved with a 2D Gaussian distribution of size $G_{size} \times G_{size}$ and the standard deviation given by σ^2 . As vectorized image is considered here for blurring operation, convolution is compensated by matrix multiplication. In general, to represent convolution as multiplication, consider a Toeplitz matrix of the form

$$T = \begin{pmatrix} T_0 & T_{-1} & \cdots & T_{2-n} & T_{1-n} \\ T_1 & T_0 & \cdots & T_{3-n} & T_{2-n} \\ \vdots & \vdots & \ddots & \vdots & \vdots \\ T_{n-2} & T_{n-3} & \cdots & T_0 & T_{-1} \\ T_{n-1} & T_{n-2} & \cdots & T_1 & T_0 \end{pmatrix} \quad (2.4)$$

Where, negative indices are used to simplify the notation.

Now define the operation $T = \text{toeplitz}(t)$ as converting a vector $t = [t_{1-n} \cdots t_1 \ t_0 \ t_1 \cdots t_{n-1}]$ (of length $2n-1$) to the form 3 as mentioned above, with the

negative indices of t corresponding to the first row of \mathbf{T} and the positive indices to the first column, with t_0 as the corner element.

Consider a $K_x K_y \times K_x K_y$ matrix T of the form

$$T = \begin{bmatrix} T_0 & T_{-1} & \cdots & T_{1-K_y} \\ T_1 & T_0 & T_{-1} & \vdots \\ \vdots & \vdots & \ddots & T_{-1} \\ T_{K_y-1} & \cdots & T_1 & T_0 \end{bmatrix} \quad (2.5)$$

Where each block \mathbf{T}_j in matrix is a $K_x \times K_y$ block matrix. This matrix is called block Toeplitz along with Toeplitz blocks (BTTB). Finally, 2D convolution can be converted to an equivalent matrix multiplication form:

$$t * f = \text{mat}(T * \text{vec}(f)) \quad (2.6)$$

Where T is the $K_x K_y \times K_x K_y$ BTTB matrix of the form (2.5) with $\mathbf{T}_j = \text{toeplitz}(t_j)$.

Here t_j denotes the j^{th} column of the $(2K_x - 1) \times (2K_y - 1)$ matrix t [19]. The blur operator matrix is denoted by B . Depending on the image source, the assumption of blur can be ignored in certain cases.

2.2.1.3. Down-sampling operator

The two-dimensional down-sampling operator discards some elements of a matrix while leaving others unchanged. In the case of down-sampling by rows operator, $D_x(r_x)$, the first row and all rows whose numbers are one plus a multiple of r_x are preserved, while all others are removed. Equivalently, the down-sampling done by columns operator $D_y(r_y)$ keeps the first column and the columns whose numbers are multiple of r_y with an increment by one, while removing others. As an example, consider the matrix

$$M_{ex} = \begin{bmatrix} 1 & 5 & 9 & 13 & 17 & 21 & 25 \\ 2 & 6 & 10 & 14 & 18 & 22 & 26 \\ 3 & 7 & 11 & 15 & 19 & 23 & 27 \\ 4 & 8 & 12 & 16 & 20 & 24 & 28 \end{bmatrix}$$

Suppose $r_x=2$, Then we have the down-sampled by rows matrix.

$$\text{mat}(D_x \text{vec}(M_{ex})) = \begin{bmatrix} 1 & 5 & 9 & 13 & 17 & 21 & 25 \\ 3 & 7 & 11 & 15 & 19 & 23 & 27 \end{bmatrix}$$

Suppose $r_x=2$, Then we have the down-sampled by columns matrix.

$$\text{mat}(D_y \text{vec}(M_{ex})) = \begin{bmatrix} 1 & 13 & 25 \\ 2 & 14 & 26 \\ 3 & 15 & 27 \\ 4 & 16 & 28 \end{bmatrix}$$

Matrices can be down-sampled by both rows and columns. In the above example,

$$\text{mat}(D_x D_y \text{vec}(M_{ex})) = \begin{bmatrix} 1 & 13 & 25 \\ 3 & 15 & 27 \end{bmatrix}$$

If we define a block matrix B_2 ,

$$B_2 = \begin{bmatrix} 1 \\ 0_{(r_x-1) \times 1} \end{bmatrix}$$

Then D_x can be written as

$$\left[\text{diag} \left(\text{rep} \left(B_2, \frac{n_x n_y}{r_x} \right) \right) \right]^T$$

For D_y ,

$$B_3 = \begin{bmatrix} I_{n_x/r_x} \\ 0_{(n_x(n_y-r_y)/(r_x r_y)) \times n_x/r_x} \end{bmatrix}$$

$$D_y = \left[\text{diag} \left(\text{rep} \left(B_3, n_y/r_y \right) \right) \right]^T \quad (2.7)$$

It should be noted that the operations of down-sampling of rows and columns commute, however, the down-sampling operators themselves do not. This is because of the requirement of matrices that must be compatible in size for successful multiplication. If the

D_x operator with size $S_x S_y / r_x \times S_x S_y$ is applied first. The D_y operator must be of size $S_x S_y / (r_x r_y) \times S_x S_y / r_x$. After construction of the above operators the order of these operators cannot be reversed.

As an example, consider a 4×4 matrix M_{ex} that is down-sampled by 2 in both directions. Its down-sampling operators are:

$$D_x = \begin{bmatrix} 1 & 0 & 0 & 0 & 0 & 0 & 0 & 0 & 0 & 0 & 0 & 0 & 0 & 0 & 0 & 0 \\ 0 & 0 & 1 & 0 & 0 & 0 & 0 & 0 & 0 & 0 & 0 & 0 & 0 & 0 & 0 & 0 \\ 0 & 0 & 0 & 0 & 1 & 0 & 0 & 0 & 0 & 0 & 0 & 0 & 0 & 0 & 0 & 0 \\ 0 & 0 & 0 & 0 & 0 & 0 & 1 & 0 & 0 & 0 & 0 & 0 & 0 & 0 & 0 & 0 \\ 0 & 0 & 0 & 0 & 0 & 0 & 0 & 0 & 1 & 0 & 0 & 0 & 0 & 0 & 0 & 0 \\ 0 & 0 & 0 & 0 & 0 & 0 & 0 & 0 & 0 & 0 & 1 & 0 & 0 & 0 & 0 & 0 \\ 0 & 0 & 0 & 0 & 0 & 0 & 0 & 0 & 0 & 0 & 0 & 0 & 1 & 0 & 0 & 0 \\ 0 & 0 & 0 & 0 & 0 & 0 & 0 & 0 & 0 & 0 & 0 & 0 & 0 & 0 & 1 & 0 \end{bmatrix}$$

$$D_y = \begin{bmatrix} 1 & 0 & 0 & 0 & 0 & 0 & 0 & 0 \\ 0 & 1 & 0 & 0 & 0 & 0 & 0 & 0 \\ 0 & 0 & 0 & 0 & 1 & 0 & 0 & 0 \\ 0 & 0 & 0 & 0 & 0 & 1 & 0 & 0 \end{bmatrix}$$

It is noticed that the down-sampling-by-columns operator (D_y) is much smaller than the down-sampling by rows operator (D_x). This is because D_y will be multiplied not with the original matrix M , but with the smaller matrix $D_x \text{vec}(M_{ex})$, or M_{ex} that has already been down-sampled by rows.

2.2.1.4. Data Model

From equations 2.1 and 2.2 in section 2.1, the observed images in matrix terms are given by:

$$y_i = DBW_i x, \quad \forall \quad i = 1, \dots, N$$

Where $D = D_x D_y$ and $W_i = W_x(d_{ix})W_y(d_{iy})$.

If we define a matrix A_i as the product of down-sampling, blurring, and shift matrices, (from equation 2.2)

$$A_i = DBW_i$$

Then the above equation can be written as,

$$y_i = A_i x, \quad \forall i = 1, \dots, N$$

Furthermore, we can obtain all of the observed frames with a single matrix multiplication, rather than N multiplications as above. If all of the vectors y_i are vertically concatenated, the result is a vector y that represents all of the LR frames. Now, the mapping from x to y is also given by the vertical concatenation of all matrices; A_i . The resulting matrix A consists of N block matrices, where each block matrix A_i operates the same vector x . By property of block matrices, the product Ax is the same as if all vectors y_i were stacked into a single vector. Hence

$$y = Ax$$

The IO model described above assumes that there is a single image that is geometrically shifted by different amounts, however, that is not the case in practical applications. Mostly, we are interested in some object which is moving while the background remains fixed while remaining in the field of view of the camera. If we consider only a few frames (which can be recorded in a fraction of a second), we can define a “bounding box” within which the object will remain for the duration of observation. In this thesis, this “box” is referred to as the region of interest (ROI). All operations need to be done only with the ROI, which is much more efficient computationally. It also sets the additional problem of determining the object's initial location and its movement within the ROI. These issues will be described in the section dealing with motion estimation [13] [14].

Also, although noise is not explicitly included in the model, the inverse model formulation (described next), assumes that additive white Gaussian (AWGN) noise, if present, can be attenuated by an optimization algorithm.

2.2.2. SR Inverse model

The purpose of the inverse model is to reconstruct an HR image given several LR frames. Since in the forward model the HR to LR transformation is done with matrix multiplication, it is logical to formulate the reconstruction problem as matrix inversion. Indeed, the purpose of transforming images into vector form and constructing matrix operators to represent translation, blur and down-sample parameters were to represent the HR-to-LR mapping in the form of Eq. 2.2, a system of linear equations.

First, it should be noted that this system may be un-determined. Typically, the combination of all available LR frames contains only a part of the information in the HR frame. Alternatively, some frames may contain redundant information (same set of pixel information). Hence, straightforward solution of the form $\hat{\mathbf{x}} = A^{-1}\mathbf{y}$ may not be feasible. Rather the optimal solution can be defined as minimizing the discrepancy between the observed and the reconstructed data in the least squares sense.

2.3. Iterative Back Projection

The iterative back-projection (IBP) technique was first proposed by Irani *et. al.* [21], can attain the High Resolution (HR) image interpolation and de-blurring simultaneously, while Its motto is that the reconstructed HR image from the degraded Low Resolution (LR) image should produce the same observed LR image if passing it through the same blurring and down-sampling process.

The IBP technique can minimize the reconstruction error by iteratively back-projecting the reconstruction error into the reconstructed image. IBP is an efficient algorithm to acquire the HR image by minimizing the norm of the reconstruction error [17][18]. With the help of given an estimate of the reconstructed HR image and a model of the imaging process, a set of simulated LR images can be generated. Each simulated LR image is compared with the actual version and then the error can be used for correcting the estimated image. In fact, it is difficult to restore a HR image in a one-shot manner. Therefore, an iterative procedure is needed. This process is iterated until some stopping condition is achieved. Generally, the minimization of some error criterion between the simulated and observed LR images is adopted as the stopping condition [22].

This method begins with an image registration procedure and iteratively refines the simulated low resolution images by subtracting the observed images from them.

First it finds a rough estimation of high resolution (HR) image called as “initial guess” X^0 and iteratively a “gradient” image is added to it during the course of operation. The gradient image i.e. calculated from the sum of the errors between each LR image and the estimated HR image [11] is given as,

$$\text{Gradient image} = (y - y^{sim}) \quad (2.8)$$

Where, y = Observed LR images

y^{sim} = Simulated LR images

These simulated LR images are compared with the observed ones and the error generated between them is back projected onto the initial guess after multiplying it with the back projection operator,

$$X = X^0 + A^{bp} (y - y^{sim}) \quad (2.9)$$

Where A^{bp} = back projection operator calculated from the imaging process

X^0 = Initial guess

X = Output High Resolution image

The algorithm considers translational, rotational, blur and down-sample operator in the back-projection matrix. The IBP technique here successfully solves the problem of blur and noise, still due to ill-posed nature of the inverse problem, the technique fails to generate a unique solution

The multi-modal optimization technique helps here in finding the more appropriate solution of $\hat{\mathbf{x}}$, because Iterative Back Projection technique being an inverse problem provides no unique solution. Therefore need of search technique to find the best solution where the mean square error of the reconstructed image is minimized.

2.4. Optimization Technique

Optimization is the process of improvisation; it is a strategy to improve the quality of the image. In other words, optimization is the mathematical process of manipulating the inputs or characteristics of a device, or an experiment to find the minimum or maximum output. The input consists of variables: the function or process is known as the cost, objective or fitness function; and the output is the minimum cost or optimum fitness.

The gradient based technique used in IBP method, updates or optimizes the HR image iteratively. The gradient based methods are normally ill-defined, because of the local optimization technique and especially not used for convex minimization problems, hence the solution it provides is either local minima or local maxima. To find the solution to multimedia problems the optimization technique should search for global minimum or global maximum.

There are different methods for solving a multi-modal optimization problem. Some of these methods are inspired from natural processes. These methods usually start with an initial set of variables and then evolve to obtain the global minimum or maximum of the objective function. Examples of such algorithms are: genetic algorithm (GA), Particle Swarm Optimization (PSO) Algorithm, Ant-Bee Colony, Simulated Annealing and Cuckoo Optimization Algorithm (COA).

The main advantages of evolutionary algorithms are:

1. Being robust to dynamic changes: Conventional methods of optimization are not robust enough to dynamic changes in the environment and they require a complete restart for providing a solution. In contrary, evolutionary computation can be used to adapt solutions to changing circumstances.
2. Broad applicability: Evolutionary algorithms can be applied to any problems that can be formulated as a function of optimization problems.
3. Hybridization with other methods: Evolutionary methods can be combined with more traditional optimization algorithms.
4. Solves problems that have no solutions: The advantage of evolutionary algorithms includes the ability to address problems for which there is no human expertise.

Even though human expertise should be used when it is needed and available; it often proves less adequate for automated problem-solving routines.

2.3.1. Cuckoo Optimization Algorithm

Figure 2.3 shows a flowchart of the proposed algorithm. Like other evolutionary algorithms, the proposed algorithm starts with an initial population of cuckoos. These initial cuckoos have some eggs to lay in some host birds' nests. Some of these eggs which are more similar to the host bird's eggs have the opportunity to grow up and become a mature cuckoo. Other eggs are detected by host birds and are killed. The grown eggs reveal the suitability of the nests in that area. The more eggs survive in an area, the more profit is gained in that area. So the position in which more eggs survive will be the term that COA is going to optimize. Cuckoos search for the most suitable area to lay eggs in order to maximize their egg survival rate [26] [27].

After remaining eggs grow and turn into a mature cuckoo, they make some societies. Each society has its habitat region to live in. The best habitat of all societies will be the destination for the cuckoos in other societies. Then they immigrate toward this best habitat. They will inhabit somewhere near the best habitat. Considering the number of eggs each cuckoo has and also the cuckoo's distance to the goal point (best habitat), some egg laying radii are dedicated to it. Then, cuckoo starts to lay eggs in some random nests inside her egg laying radius. This process continues until the best position with maximum profit value is obtained and most of the cuckoo population is gathered around the same position.

Nomenclature:

- Cuckoo : new iteration
- Nest : solution
- ELR (Egg Laying Range) : Lower and Upper boundary to limit the Levy flights
- Eggs : initial guess

Here Levy flights follow Mantegna's algorithm which decides the step size of Cuckoo's each flight to find a nest for laying an egg.

The step size calculation is as shown below:

$$\text{step length} = \frac{u}{|v|^{\frac{1}{\beta}}} \quad (2.10)$$

Where, u and v are estimated from normal distributions *i.e.*:

$$u \sim N(0, \sigma_u^2); v \sim N(0, \sigma_v^2)$$

Where σ_u^2 & σ_v^2 are given by,

$$\sigma_u = \left\{ \frac{(1+\beta) \sin \frac{\pi\beta}{2}}{\left[\frac{(1+\beta)}{2} \right] \beta 2^{\frac{\beta-1}{2}}} \right\}^{\frac{1}{\beta}} \quad (2.11)$$

$$\sigma_v = 1 \quad (2.12)$$

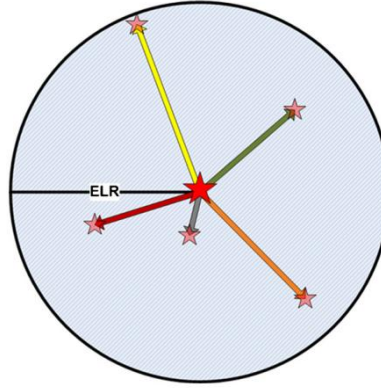


Figure 2.3: Random egg laying in ELR, central red star is the initial habitat of the cuckoo with 5 eggs; pink stars are the eggs' new nest.

The cuckoo optimization algorithm is described in a flow chart in figure 2.4

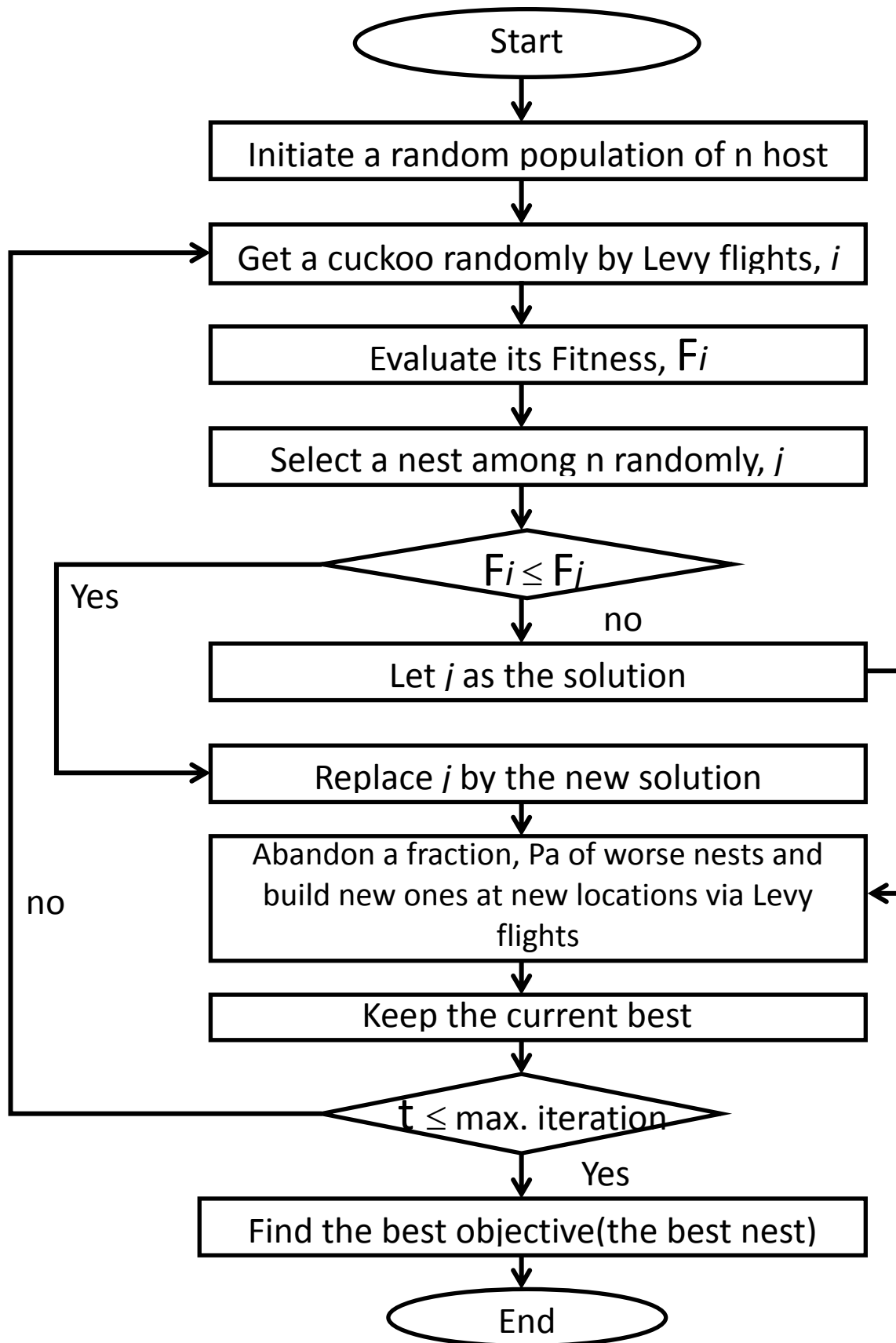


Figure 2.4: Flow chart of conventional Cuckoo Optimization Algorithm.

Chapter 3

Simulations and Result Analysis

3.1. Simulations

In this thesis we have done the super resolution reconstruction experiments using the proposed algorithm. For simplicity, and to have a formal metric for comparisons, most of the image sequences considered are synthetic, *i.e.* they were artificially generated from existing images for testing. The images are photographs taken in real time, assumed here as the “HR original” and the aim of our Super Resolution Reconstruction problem is to attain the quality of HR original. However, the improvement of HR images from the LR ones so good that it can be seen visually.

The proposed algorithm is compared with already existing gradient based method. The resolution enhancement methods which are used to compare are Bicubic interpolation, Iterative Back Projection [11] and, the proposed algorithm, IBP with Cuckoo Optimization Algorithm.

Figure 3.1 shows side by side comparison of LR and HR images. The HR image (3.1b) was reconstructed from 9 LR image portions (3.1a), here both of the images are shown at the same scale.

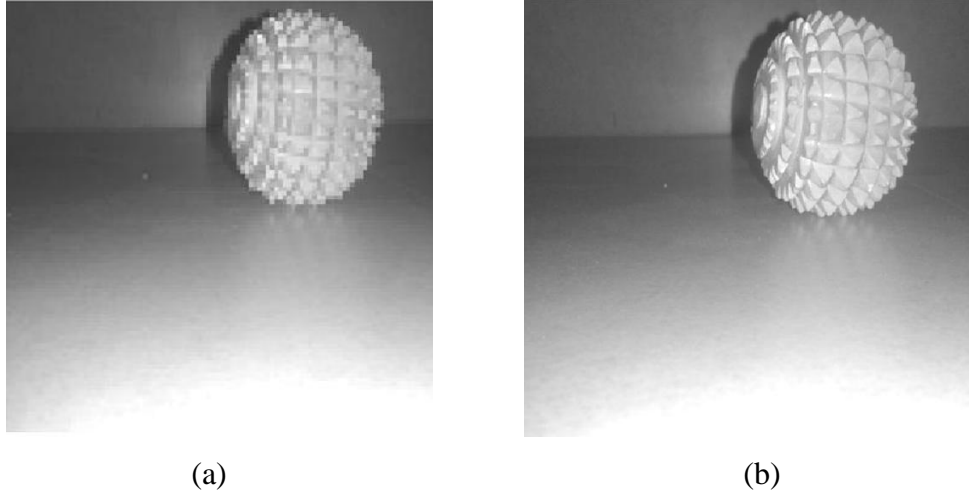


Figure 3.1: (a) LR Image, (b) HR image, where both of the images are shown in same scale

3.2. Simulations using Synthetic data

The forward model for super-resolution reconstruction problem as described in Section 2.2.1 is used to generate the synthetic super-resolution datasets. Image intensities are all in the range $\left(-\frac{1}{2} \text{ to } +\frac{1}{2}\right)$, we have converted the acquired images into grayscale. The Point Spread Function (PSF) used is a Gaussian kernel with a standard deviation of 0.25 low resolution pixels this resolution enhancement process provides a zoom factor of 2 in both X and Y direction, *i.e.* a four time area increment going from low to high resolution. The simulations are done with MATLAB R2012a (version 7.14).

Fig 3.2(a) shows a photograph of an Accu-pressure ball taken with SAMSUNG GT-7562 mobile camera of 5MP resolution. The color photograph then converted to grayscale and resized to (512×512) pixels to be considered as our reference image shown in fig. 3.2(b).

From the reference figure 3.2(b) 4 number of simulated LR images, of size (256×256) , are formed using the forward model as discussed in section 2.1.1, the LR images are shown in figure 3.2(c-f). Each of the LR image is geometrically warped while images 3.2(c-e) are translated using different offsets the last LR image, 3.2(f), has rotational affine transform. Along with geometric warping LR images are the result of blur and down-sample operators.

Figure 3.2(g) shows the bicubic interpolation of one of the LR images. Here we are using bicubic interpolation, simply because of its superiority to bilinear and nearest neighborhood interpolation method. It creates the output matrix by replacing each input pixel value with the weighted average of the two translated values on either side and thus addition of new rows and columns to older image.

Figure 3.2(h) shows the Super resolution image with IBP. The gradient based method takes four of the LR images Fig. 3.2(c-f) as input along with translation, blur and down-sample operator information, then solves the equation 2.9 iteratively. The mean square error of this image as compared to reference image is 0.0027 and SSIM index is 0.9982.

Figure 3.2(i) shows Super resolution output with IBP and Cuckoo optimization algorithm. As the optimization algorithm requires, 10 numbers of solutions are imported from the IBP iterations to form the nests. Since the performance of the optimization

technique depends on its initial guess, the best 10 solutions of IBP iterations are passed to Cuckoo search technique.

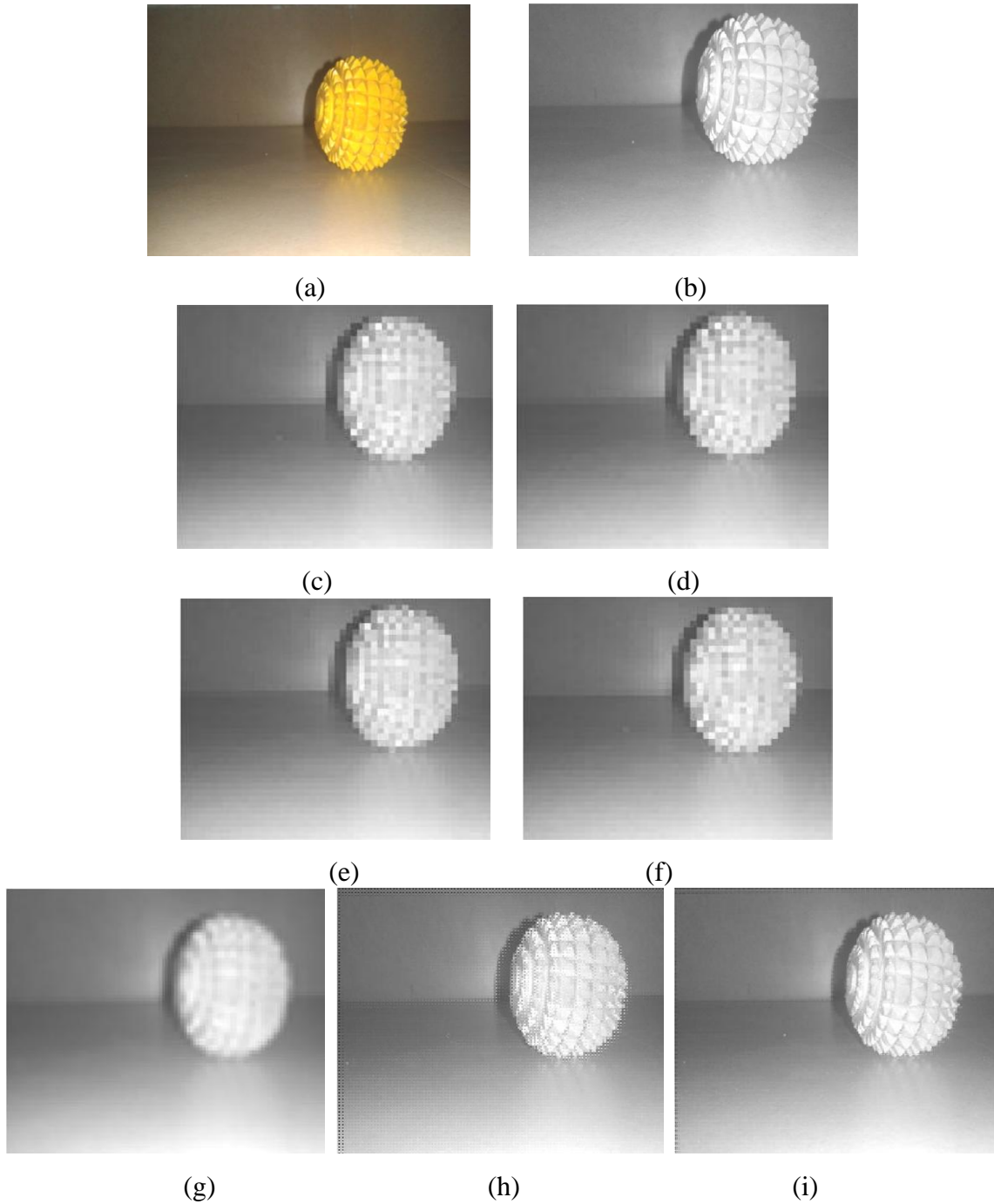


Figure 3.2(a-i): (a) color image captured by the SAMSUNG GT-S7562 camera, (b) after resizing the previous image with 512×512 resolution, (c-f) shows 4 low resolution images each with unique information, (g) bicubic interpolation of one of the LR image, (h) Super resolution solution using IBP method and (i) super resolved HR image from IBP and Cuckoo optimization algorithm.

Then cuckoo search for the best nest starts as discussed in section 2.3.1. The mean square error of this image as compared to reference image is 0.0016 and SSIM index is 0.9999, the terms mean square error and SSIM are discussed in section 3.3.1 and 3.3.2 respectively.

Fig. 3.3 shows a (256×256) pixel ground truth image, which is accompanied by four corresponding (102×102) pixel low-resolution images generated from the ground truth images at half the resolution. In no cases do the areas of the images used for the prior overlap with the sections used in generating the datasets, therefore each low resolution image provides unique information to the super-resolution technique.

Fig. 3.3.1 shows a (256×256) pixel ground truth image, which is accompanied by three corresponding (102×102) pixel low-resolution images and a rotated image generated from the ground truth images at half the resolution. The introduction of a small angle in one of the LR images causes the results to be more distorted as compared to figure 3.3 (f,g).

The resolution enhancement from low resolution to high resolution is clearly visible from the above images. The eye area in 3 of the images in fig. 3.3 is highlighted to show, how the details got improved in Super resolution technique than interpolation method.

Fig.3.4 shows a (256×256) pixel ground truth image, each accompanied by nine corresponding (102×102) pixel low-resolution images generated from the ground truth images at half the resolution. In no cases do the areas of the images used for the prior overlap with the sections used in generating the datasets, therefore each low resolution image provides unique information to the super-resolution technique.

The resolution enhancement in 9 LR images case is much better than 4 LR images case. It is because the more number of LR image provides more information about the scene in the image.

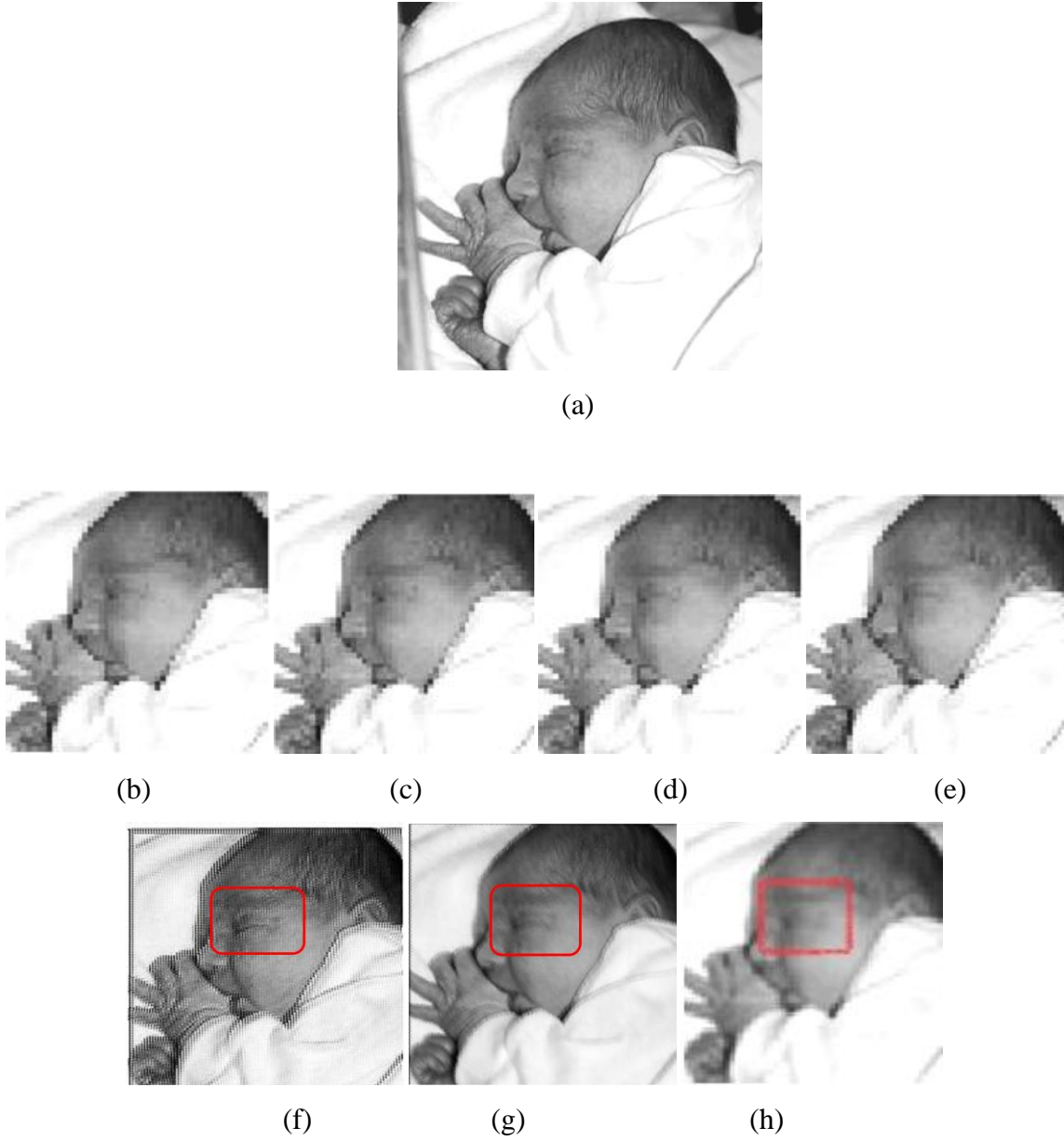


Figure 3.3: Image data for the “Baby” example. (a) Ground truth for the baby image. (b-e) Four of the low-resolution images generated as synthetic inputs for super-resolution technique. (f) HR image reconstructed using SR Iterative Back Projection method; (g) HR image reconstructed using the SR IBP method along with Cuckoo Optimization Algorithm; (h) Bicubic interpolation.

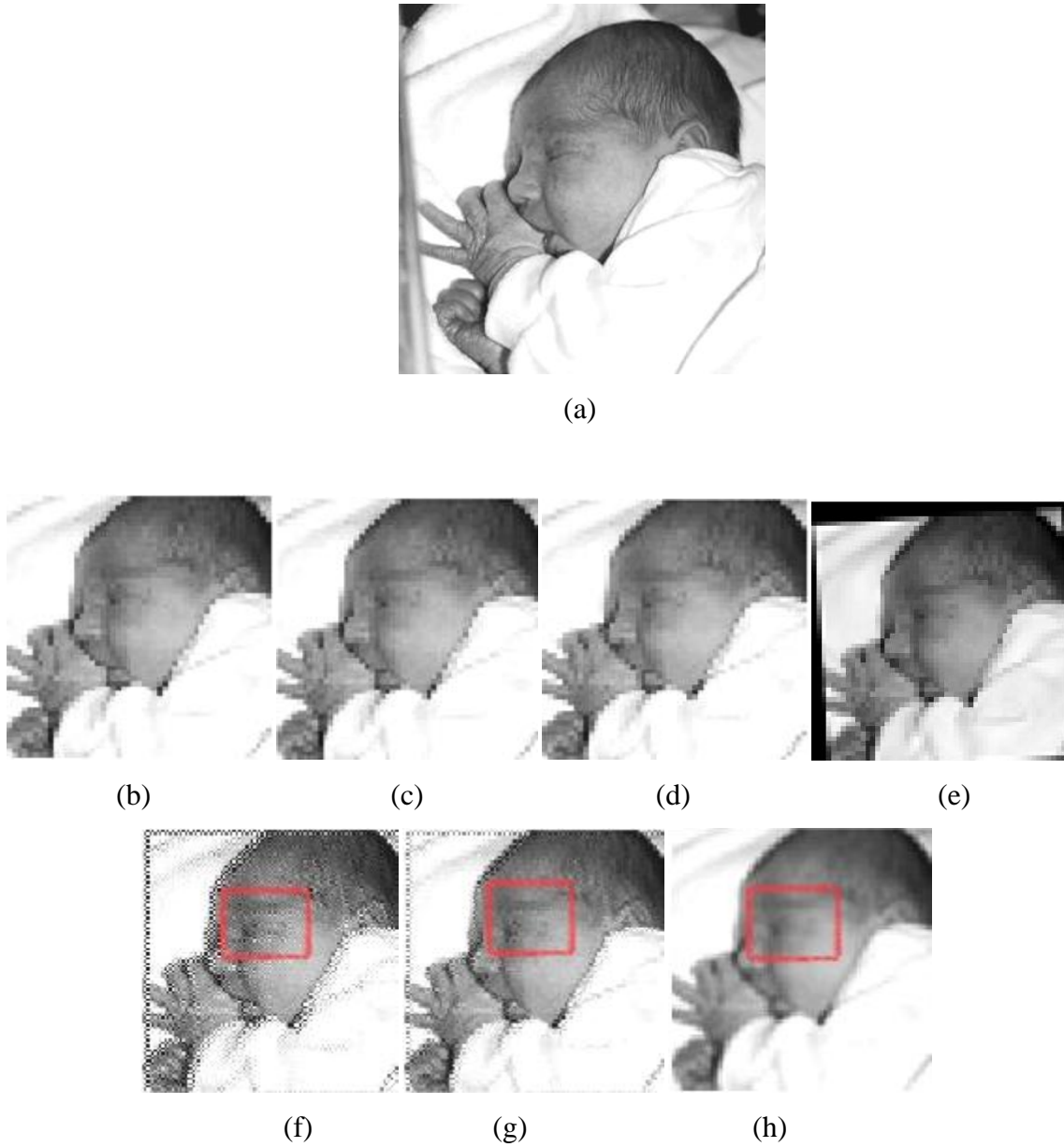


Figure 3.3.1: Image data for the “Baby” example. (a) Ground truth for the baby image. (b-d) Three of the low-resolution images generated as synthetic inputs for super-resolution technique. (e) a low-resolution image rotated anti-clockwise with a very small angle. (f) HR image reconstructed using SR Iterative Back Projection method; (g) HR image reconstructed using the SR IBP method along with Cuckoo Optimization Algorithm; (h) Bicubic interpolation.

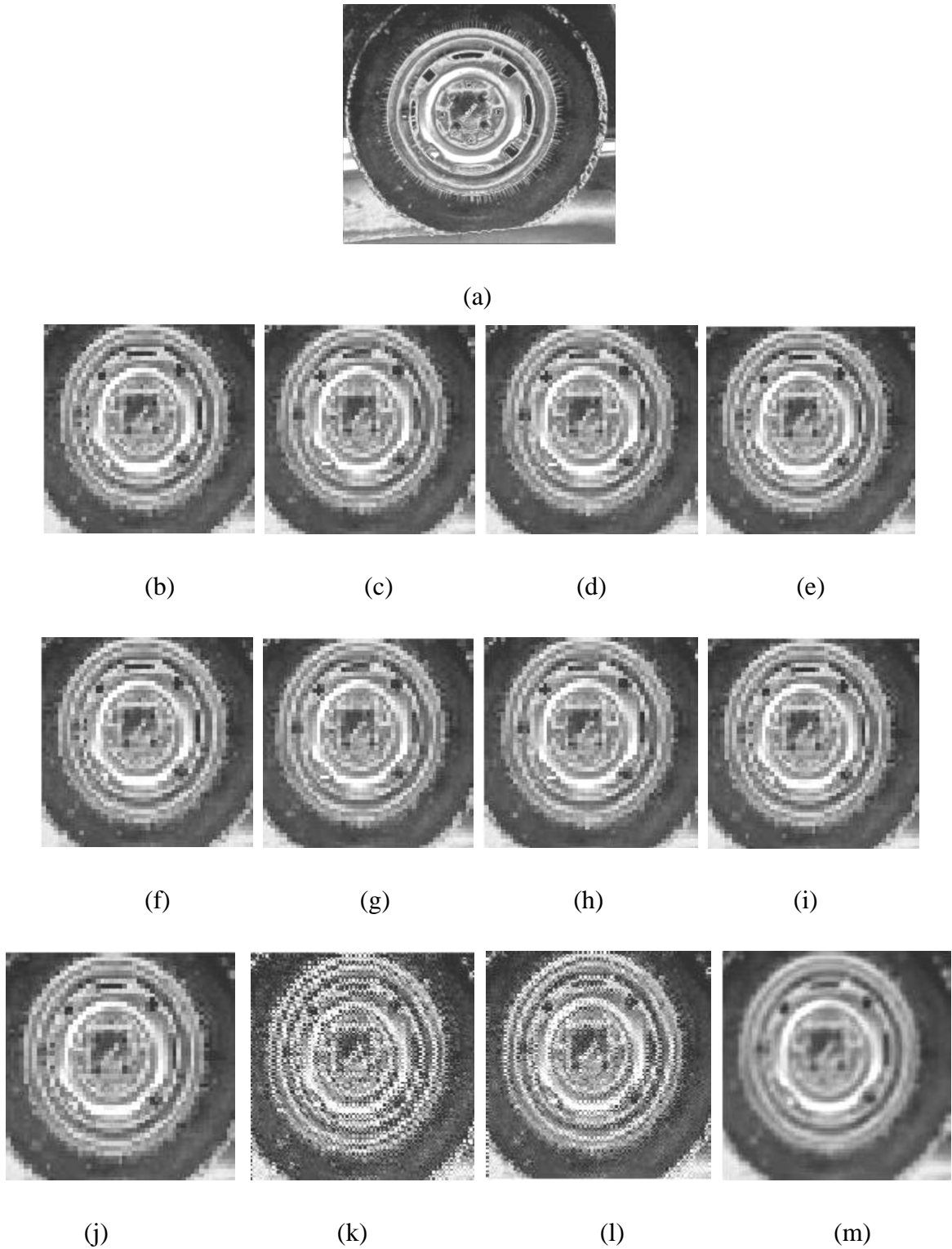


Figure 3.4: Image data for the “Wheel” example (a) The ground truth wheel image. (b-j) Four of the low-resolution images generated as synthetic inputs for super-resolution technique. (k) HR image reconstructed using SR Iterative Back Projection method, (l). HR image reconstructed using the SR IBP method along with Cuckoo Optimization Algorithm, (m) Bicubic interpolation.

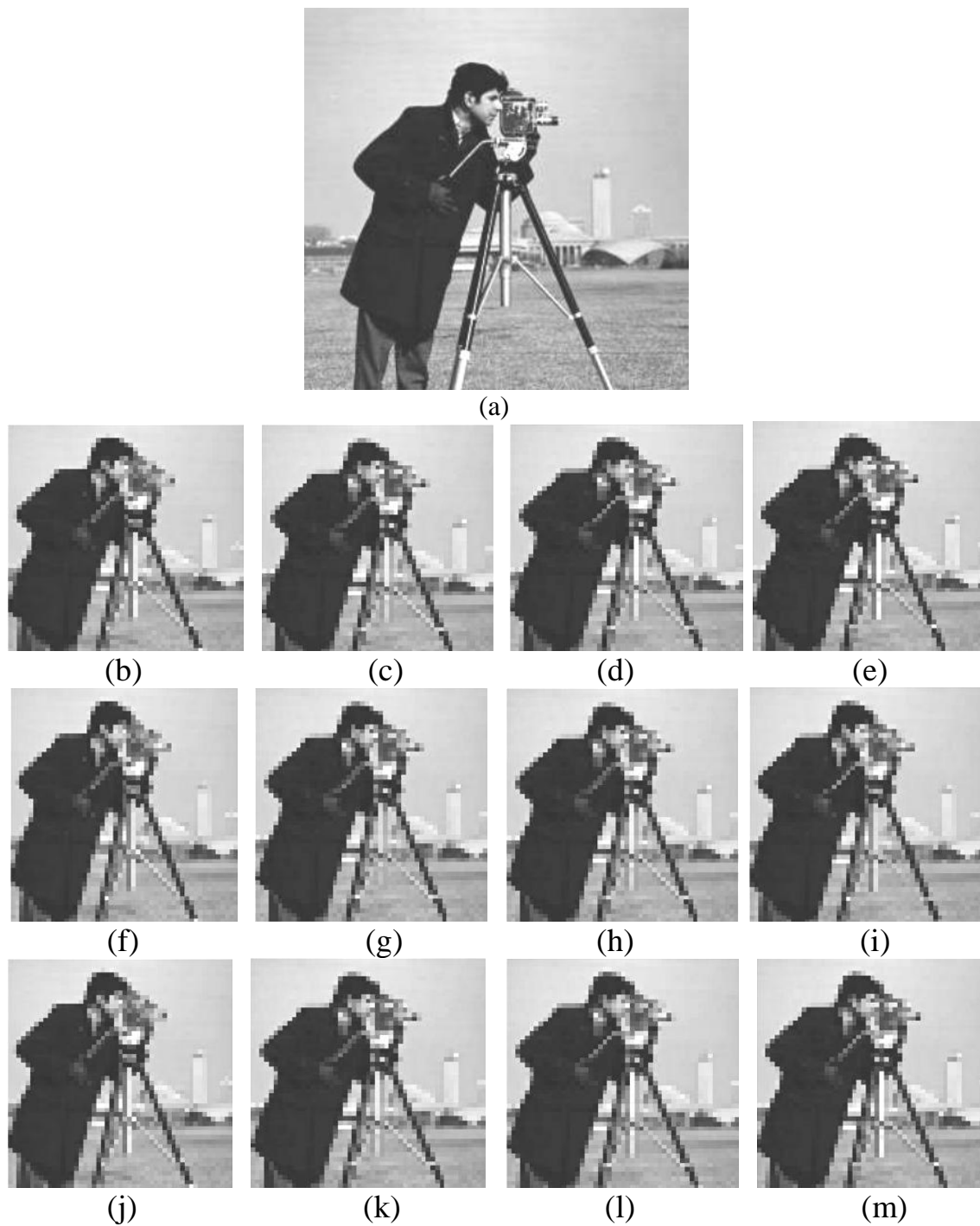


Figure 3.5: Image data for the “camera man” example (a) The ground truth camera man image. (b-m) First twelve of sixteen low-resolution images generated as synthetic inputs for super-resolution technique.

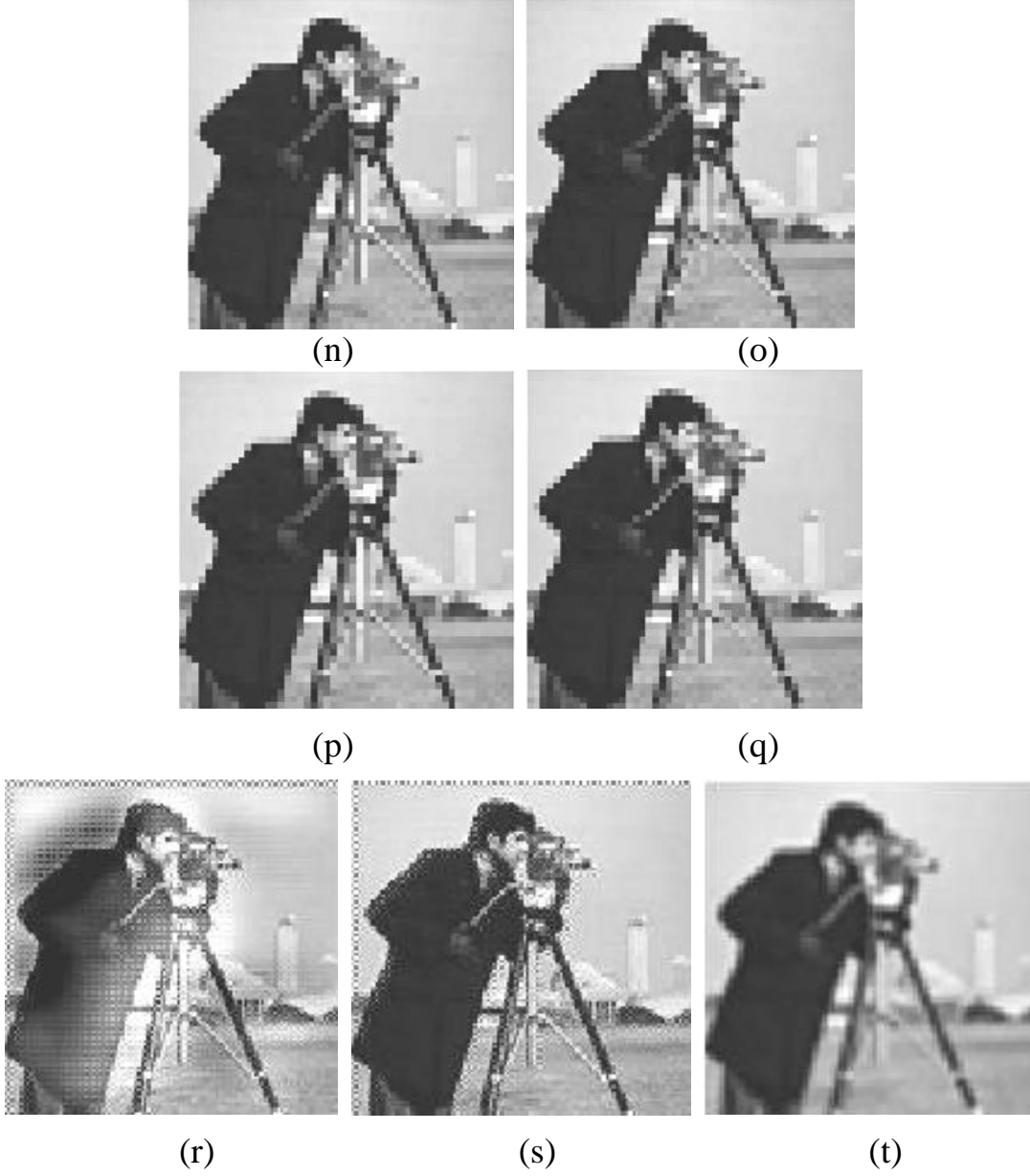


Figure 3.5: *(n-q) Low-resolution images generated as synthetic inputs for super-resolution technique. (r) HR image reconstructed using SR Iterative Back Projection method. (s) HR image reconstructed using the SR IBP method along with Cuckoo Optimization Algorithm. (t) Bicubic interpolation.*

Figure 3.5 shows a (256×256) -pixel ground truth images, each accompanied by 16 corresponding (102×102) pixel low-resolution images generated from the ground truth images at half the resolution. In no cases do the areas of the images used for the prior overlap with the sections used in generating the datasets, therefore each low resolution image provides unique information to the super-resolution technique.

3.3. Image quality Assessment

Any processing applied to an image may cause an important loss of information or quality. Image quality evaluation methods can be subdivided into objective and subjective methods [29]. Subjective methods are based on human judgment and operate without reference to explicit criteria. Objective methods are based on comparisons using explicit numerical criteria [30].

Image quality is a feature of an image that measures the perceived image degradation (typically, compared to an ideal or perfect image). Imaging systems may have introduced some amount of distortion or artifacts in the 2D-signal, therefore the quality assessment is an important problem. The metrics that have been used in this thesis for the image quality assessment (IQA) are discussed in the subsequent sections.

3.3.1. Mean Square Error

The mean square error (MSE) between two images $g(n, m)$ and $\hat{g}(n, m)$ can be given as;

$$E_{MSE} = \frac{1}{MN} \sum_{n=1}^N \sum_{m=1}^M [\hat{g}(n, m) - g(n, m)]^2 \quad (3.1)$$

One problem with MSE is that it depends strongly on the image intensity scaling. A mean-square-error of 100.0 for an 8-bit image (with pixel values in the range 0-255) looks alarming; but a MSE of 100.0 for a 10-bit image (pixel values in [0, 1023]) is barely noticeable.

3.3.2. SSIM

The Structural SIMilarity (SSIM) index is a method for measuring the similarity between two images [31]. The SSIM index can be considered as a quality measure of one of the images being compared provided the other image (or reference image) is regarded as of perfect quality. The SSIM index is a full reference metric, in other words, the image quality measurement is based on an initial distortion-free image as reference. SSIM is designed to improve on traditional methods like mean squared error, which has proved to be inconsistent with human eye perception. The difference with respect to other technique mentioned previously such as MSE, is that the approach estimate perceived errors on the other hand SSIM considers image degradation as perceived change in structural information. Structural

information is the idea that the pixels have strong interdependencies especially when they are spatially close. These dependencies carry useful information about the structure of the objects in the visual scene [31].

At a high level, SSIM attempts to measure the change in luminance, contrast and structure in an image. Luminance is modeled as average pixel intensity, contrast by the variance between the reference and distorted image, and structure by the cross-correlation between the 2 images. The resulting values are combined (using exponents referred to as alpha, beta, and gamma) and averaged to generate a final SSIM index value.

The general form of SSIM can be given as:

$$SSIM(x, y) = [l(x, y)]^\alpha [c(x, y)]^\beta [s(x, y)]^\gamma \quad (3.2)$$

Where, $\alpha > 0$, $\beta > 0$ and $\gamma > 0$ are parameters used to adjust the relative importance of the three components, and x, y are image patches, and

$$l(x, y) = \frac{2\mu_x\mu_y + C_1}{\mu_x^2 + \mu_y^2 + C_1} \quad (3.3)$$

$$C(x, y) = \frac{2\sigma_x\sigma_y + C_2}{\sigma_x^2 + \sigma_y^2 + C_2} \quad (3.4)$$

$$S(x, y) = \frac{\sigma_{xy} + C_3}{\sigma_x\sigma_y + C_3} \quad (3.5)$$

$l(x, y)$ in equation 3.3 is luminance comparison, $C(x, y)$ in equation 3.4 is contrasted comparison and $S(x, y)$ in equation 3.5 is structural comparison. C_1, C_2 and C_3 are the constants avoiding instability. μ_x and μ_y are mean average of x and y . σ_x^2 and σ_y^2 are variance of x and y , σ_{xy} is the covariance of x and y . In order to simplify the equation 3.2 set $\alpha = \beta = \gamma = 1$ and,

$$C_1 = (K_1 L)^2$$

$$C_2 = (K_2 L)^2$$

$$C_3 = C_2/2$$

Where L is the dynamic range of the pixel values (255 for 8-bit grayscale images), and

$K_1, K_2 \ll 1$ is a small constant. Therefore equation 3.2 can be re-written as,

$$SSIM(x, y) = \frac{(2\mu_x\mu_y + C_1)(2\sigma_{xy} + C_2)}{(\mu_x^2 + \mu_y^2 + C_1)(\sigma_x^2 + \sigma_y^2 + C_2)} \quad (3.6)$$

Here we have kept the value of constants in equation 3.6 as $C_1 = 0.07, C_2 = 0.07$, dynamic range of the image is $L = 255$ and local window taken is of size 8 by 8 with each element value as 1.

The test images used for validation are:



(a)



(b)



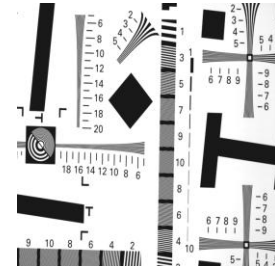
(c)



(d)



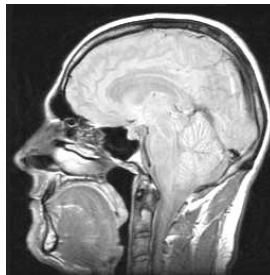
(e)



(f)



(g)



(h)



(i)



(j)

Figure 3.6: shows the test images used here for assessment of quality of the super resolved image. (a) Tier, (b) Pout, (c) “Deer”, (d) “Baby”, (e) “Blocks”, (f) “Scale”, (g) “Kids”, (h) “brain MRI”, (i) “Satellite”, (j) “Camera Man” image

Blur $\sigma=0.2500$ Sl. No. of Images	No. of LR Images used	Mean Square Error		SSIM	
		IBP	IBP+COA	IBP	IBP+COA
1	4	0.0074	0.0073	0.9999	0.9999
	9	0.0036	0.0032	0.9999	0.9999
	16	0.0021	0.0021	1.0000	1.0000
2	4	0.0463	0.0097	0.9994	0.9999
	9	0.0227	0.0116	0.9998	0.9999
	16	0.0041	0.0039	1.0000	1.0000
3	4	0.0131	0.0092	0.9998	0.999
	9	0.0068	0.0049	0.9999	0.9999
	16	0.0122	0.0040	0.9998	0.9999
4	4	0.0058	0.0020	0.9999	1.0000
	9	0.0039	0.0023	1.0000	1.0000
	16	Not converging	0.0016	Not converging	1.0000
5	4	0.0819	0.0233	0.9983	0.9995
	9	0.0090	0.0087	0.9998	0.9998
	16	Not converging	0.0038	Not converging	0.9999
6	4	0.0481	0.0190	0.9992	0.9997
	9	0.0132	0.0091	0.9998	0.9999
	16	0.0356	0.0057	0.9993	0.9999
7	4	0.0126	0.0124	0.9998	0.9998
	9	0.0112	0.0110	0.9998	0.9998
	16	0.0090	0.0071	0.9999	0.9999
8	4	0.0090	0.0048	0.9998	0.9999
	9	0.0063	0.0043	0.9999	0.9999
	16	Not converging	0.0070	Not converging	0.9999
9	4	0.0306	0.0113	0.9997	0.9999
	9	0.0079	0.0077	0.9999	0.9999
	16	Not converging	0.0077	Not converging	0.9999
10	4	0.0870	0.0533	0.9984	0.9994
	9	0.0255	0.0243	0.9996	0.9996
	16	Not converging	11.0389	Not converging	0.9684

Table 3.1: MSE and SSIM index of test images of size (128×128) with 4, 9 and 16 LR images correspond to IBP only and (IBP+COA) algorithm.

3.3.3. Result Analysis

In simulation, set of ten test images of size (128×128) are considered for validating the proposed algorithm. For confirmation of proposed algorithm mean square error and SSIM index are calculated using formula 3.1 and 3.6 respectively. The error indexes are calculated for reconstructing an HR image with respect to reference image using IBP only and (IBP+COA) algorithm. These calculations are repeated for 4, 9 and 16 number of LR images. The results are shown in table no. 3.1. The enhancement of HR reconstructed image from corresponding LR images is much better which is clearly visible from figures 3.1 to 3.6.

The tabulation of simulated results in table no. 3.1 clearly shows the improvement in HR solutions with IBP+COA method than only IBP. It is because of random walks used in COA instead of constant gradients as in IBP method.

For each test image as we increase the no. of LR images at the input side of forward model the performance of both the technique increases. But for 16 LR case it can be observed that 4 of the test images failed to converge for IBP technique, whereas results of IBP+COA method are better for all of the test images. Even the result of the 16 LR image case is better than their 9LR image counterparts, it is possible because of the multi-modal nature of the CO algorithm.

To visualize and compare the error level and SSIM index of both of the techniques we have plotted the above information into two graphs each for 4, 9 and 16 Low Resolution images.

For 4 LR inputs to the reconstruction model; Figure 3.7(a) shows serial number of images along X axis and mean square error Y axis. Here, the red line represents the mean square error of HR images which are generated using simple Iterative Back Projection (IBP) method while the blue line represents the mean square error of HR images which are generated using IBP and Cuckoo Optimization Algorithm. The mean square error compares the quality of the reconstructed image with a reference image taken using the equation 3.1 as described in section 3.3.1.

Figure 3.7 (b) shows the serial number of images along X axis and SSIM index along Y axis. Here, the red line represents the SSIM Index using simple IBP method while the green line represents the SSIM Index using IBP and Cuckoo Optimization Algorithm. The SSIM index compares SSIM between reference image and HR reconstructed image using both of the methods using the equation 3.6 as described in section 3.3.2.

For 9 LR inputs to the reconstruction model; Figure 3.8(a) shows serial number of images along X axis and mean square error Y axis. Here, the red line represents the mean square error using simple Iterative Back Projection (IBP) method while the blue line represents the mean square error using IBP and Cuckoo Optimization Algorithm.

Figure 3.8(b) shows the serial number of images along X axis and SSIM along Y axis. Here, the red line represents the SSIM using the simple IBP method while the green line represents the SSIM using IBP and Cuckoo Optimization Algorithm.

For 16 LR inputs to the reconstruction model; In Figure 3.9(a) the graph shows the serial number of images along X axis and mean square error Y axis. Five of the test images could not converge to a unique solution when IBP only is used; hence we have assumed their mean square error to be 0.05 so that the visualization of graph is improved. The red line in the graph represents the MSE using simple IBP method while the blue line represents the MSE using IBP and Cuckoo Optimization Algorithm.

The next graph, in figure 3.9(b), shows the serial number of images along X axis and SSIM index along Y axis. With the similar case as above, the SSIM index for five of the images comes nearly 0, hence to visualize the Y-scale clearly the SSIM index of non-converging images are assumed to 0.98. Here, the red line represents the SSIM Index using simple IBP method while the green line represents the SSIM Index using IBP and Cuckoo Optimization Algorithm.

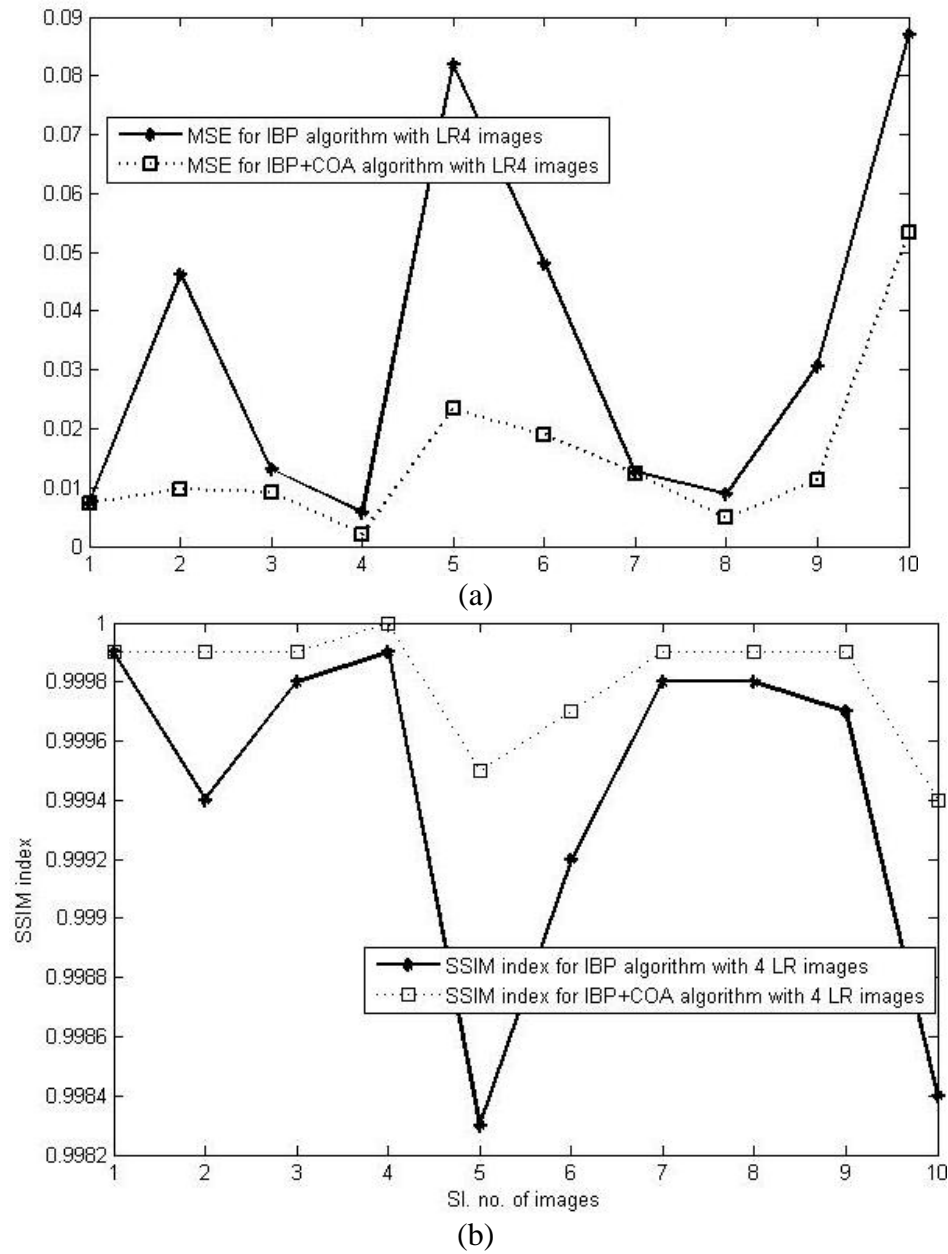


Figure 3.7: Comparison with 4 number of LR images at input, (a) mean square error values for SR IBP generated HR image and SR IBP+COA generated HR images, (b) SSIM index for SR IBP generated HR image and SR IBP+COA generated HR images.

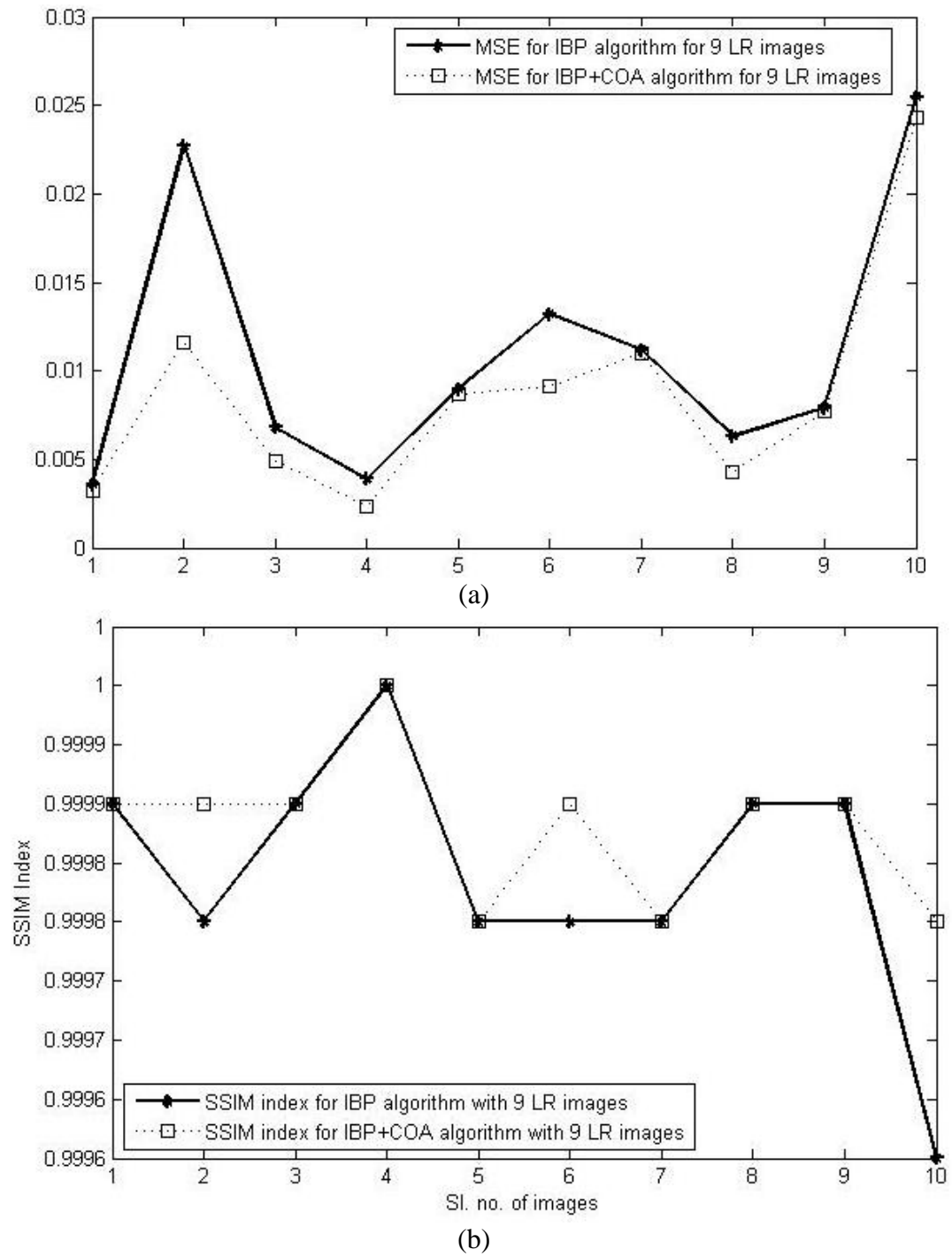


Figure 3.8: Comparison with 9 number of LR images at input, (a) mean square error values for SR IBP generated HR image and SR IBP+COA generated HR images, (b) SSIM index for SR IBP generated HR image and SR IBP+COA generated HR images.

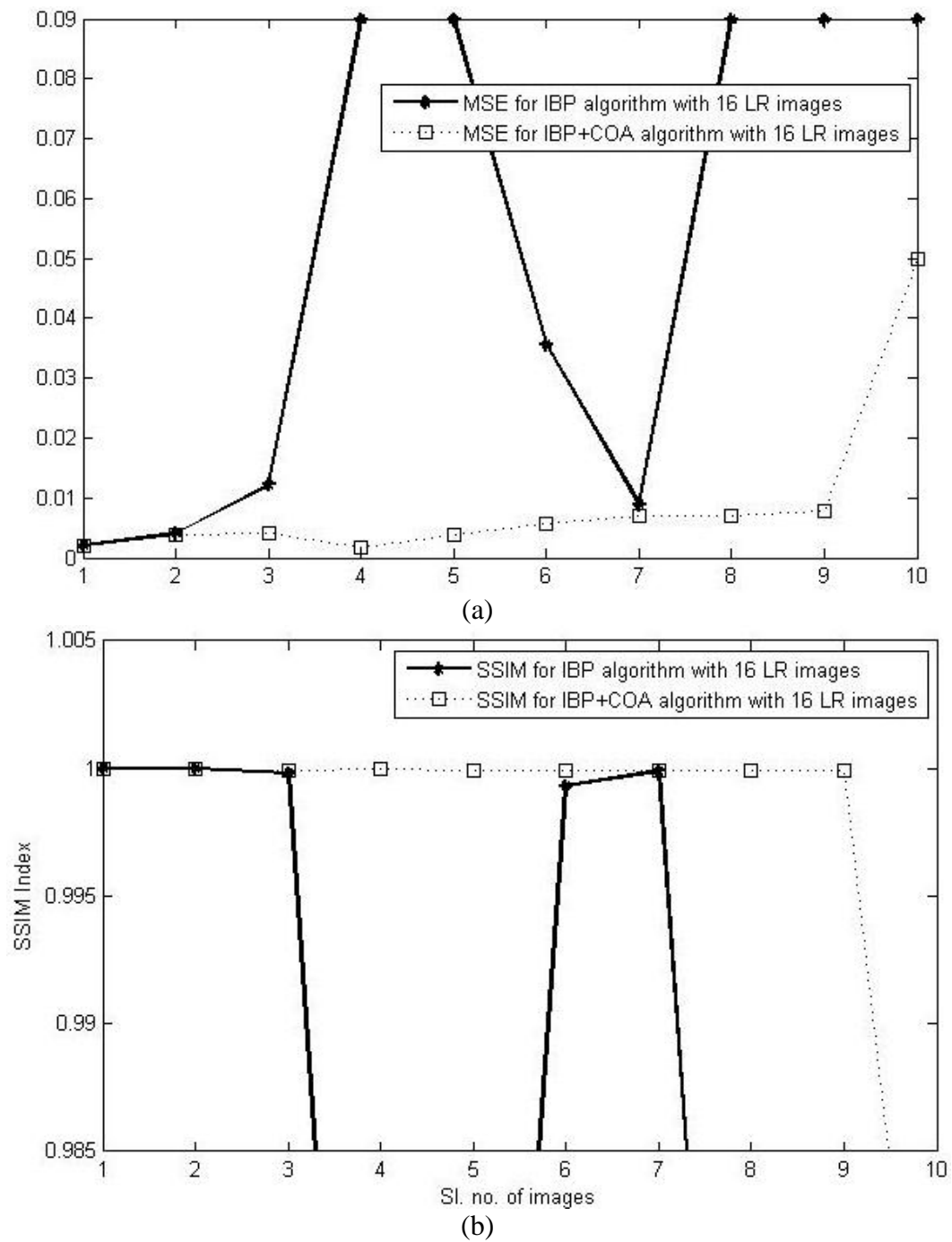


Figure 3.9: Comparison with 16 numbers of LR images at input, (a) mean square error values for SR IBP generated HR image and SR IBP+COA generated HR images, (b) SSIM index for SR IBP generated HR image and SR IBP+COA generated HR images.

Chapter 4

Conclusion & Future Research

4.1 Conclusion

In this piece of work, the problem of multiple LR image super resolution reconstruction with evolutionary optimization technique is considered. We have developed a matrix-based framework for obtaining an HR image from LR images or a sequence of displaced frames. The model describes the image degradation process in terms of matrix operations. The basic matrix blocks used here are geometric warp, down-sampling, and sensor blur operators. It is shown that the degradation process can be performed as a single matrix-vector multiplication. Then, the inverse process that reverses the image degradation is described mathematically with the aid of iterative back projection and cuckoo optimization algorithms, which accomplishes an acceptable compromise between fidelity and sharpness of the image and the presence of undesirable artifacts. The feasibility of the model is shown theoretically, experimentally via MATLAB simulation tool, and experiments with real and synthetic data.

The problem of back projection, which is critical for aligning the LR images to merge them into one, is also addressed in this thesis. The method proposed here uses the well known techniques of phase correlation and gradient constraint to achieve sub-pixel accuracy while being applicable to sub-pixel shifts. We implemented a method for improving the accuracy of back projection by cuckoo search, where the initial nests are taken from IBP estimates. The beginning of iteration *i.e.* the cuckoo flight for the best nest is governed by Lévy flights.

The results obtained using cuckoo search is better than the gradient based method. It is because of two reasons; First, cuckoo optimization uses random walk unlike IBP where constant gradient is used, while constant gradient has more chance to lose the best solution, the use of levy distribution for random walks give better result. Second, IBP method depends on single initial - guess and iteratively updates it with a constant gradient whereas COA starts with multiple initial-guesses then randomly selects one of them to start the iterations and

after iteration it updates the initial guess using Lèvy distribution. In back projection technique the solution also depends on the quality of the initial guess taken; sometimes the algorithm fails to converge when the initial - guess is of poor quality, whereas for cuckoo search multiple initial-guesses are taken from previous IBP iterations.

In this thesis work, also we conclude that with the increase in number of LR images in image observation model the quality of HR solution increases. In table no. 3.1 it is analyzed that for each test image MSE decreases with increase in no. of LR images, but some of the solutions of IBP method failed to converge, it is another advantage of COA that it always converges because of the multimodal nature of the optimization technique.

All methods and algorithms discussed in the thesis have been tested with both synthetic and real data. Super-resolution techniques can be applied to a variety of problems, practically anywhere where imaging or computer vision is involved. However, an important application, in particular, is for medical and satellite imaging.

4.2 Future work directions

The contribution of this thesis is; SR reconstruction with geometric translation, sensor blur and down-sampling information from multiple LR images and optimization of the solution.

- The results can be improved with additional edge information restored from noisy LR images, using high pass filters in parallel to back projection and optimization algorithm will help in higher frequency information in HR image.
- The SR image reconstruction can further be extended to time domain, where motion blur, motion vector, time frame factor *etc.* are considered for both spatial and temporal resolution enhancement of a video.

Bibliography

- [1] Flohr, Thomas G., et al. "Multi-Detector Row CT Systems and Image-Reconstruction Techniques", *Radiology* vol. 235 no.3, pp. 756-773, 2005.
- [2] Barceló, Juan A., Maurizio Forte, and Donald H. Sanders, eds. Virtual reality in archaeology. *Oxford, UK: Archaeopress*, 2000.
- [3] T. Komatsu, K. Aizawa, T. Igarashi and T. Saito, "Signal Processing based method for acquiring very high resolution image with multiple cameras and its theoretical analysis", *IEEE Proceedings on communications, Speech and Vision*, Vol. 140, no. 1, pp. 19-24, February 1993.
- [4] Park, Sung Cheol, Min Kyu Park, and Moon Gi Kang. "Super-resolution image reconstruction: a technical overview." *IEEE Signal Processing Magazine*, vol.20, no.3, pp. 21-36, 2003.
- [5] Farsiu, Sina, "Advances and challenges in super-resolution", *International Journal of Imaging Systems and Technology*, vol.14, no.2, pp. 47-57, 2004.
- [6] Papoulis, A. "Generalized sampling expansion". *IEEE Trans. Circuits Systems*, CAS-24, pp.652-654, 1977.
- [7] Huang, T. and Tsai, R. "Multi-frame image restoration and registration", *Advances in Computer Vision and Image Processing*, vol. 1, pp. 317-339, 1984.
- [8] Kim, S. P., Bose, N. K., and Valenzuela, H. M., "Re-cursive reconstruction of high-resolution image from noisy undersampled frames." *IEEE Trans. Acoust., Speech and Sign. Proc.*, vol. 38 pp. 1013-1027, 1990.
- [9] Ur, H. and Gross, D. "Improved resolution from subpixel shifted pictures". *Graphical Models and Image Processing*, vol. 54, no. 2, pp. 181-186, 1992.
- [10] Wang, Yanfei. "Optimization and regularization for computational inverse problems and applications". *Springer*, 2011.
- [11] M. Irani and S. Peleg, "Improving resolution by image registration", *Graphical Models and Image Processing*, vol. 53, pp.231-239, 1991.
- [12] Keren, D., Peleg, S., and Brada, R. "Image sequence enhancement using sub-pixel displacements". *IEEE Conf. on Computer Vision and Pattern Recognition*, pp. 742-746, 1988.

- [13] Baker, Simon, and Takeo Kanade. "Limits on super-resolution and how to break them", *IEEE Transactions on Pattern Analysis and Machine Intelligence*, vol. 24 no.9, pp.1167-1183, 2002.
- [14] Zomet, Assaf, and Shmuel Peleg. "Super-resolution from multiple images having arbitrary mutual motion", *Super-Resolution Imaging*, pp.195-209, 2002.
- [15] Milanfar, Peyman. Super-resolution imaging. Vol. 1. CRC Press Llc, 2010.
- [16] Elad Michael, and Arie Feuer. "Super-resolution reconstruction of image sequences", *IEEE Transactions on Pattern Analysis and Machine Intelligence*, vol.21 no.9, pp. 817-834, 1999.
- [17] Marcia L. S. Agüena, Nelson D. A. Mascarenhas, "Generalization of Iterative Restoration Techniques for Super-Resolution", *UFSCar - Universidade Federal de Sao Carlos Sao Carlos, SP – Brazil*, 2011
- [18] Siddique, Muhammad, "Performance Evaluation of Super -Resolution Reconstruction Algorithms Based On Linear Magnifications ", 2012.
- [19] Curtis R. Vogel, Computational Methods for Inverse Problems, *SIAM*, 2002.
- [20] Foroosh H., Zerubia, J.B. Berthod, Marc, "Extension of phase correlation to subpixel registration" , *IEEE Transactions on Image Processing*, vol.11, no.3, pp.188-200, Mar 2002.
- [21] M. Irani and S. Peleg, "Motion analysis for image enhancement: resolution, occlusion, and transparency", *Journal of Visual Communication and Image Representation*, vol. 4, no.4, pp. 324-335, Dec.1993.
- [22] G. Lin and M. Lai, "Enhancing resolution using iterative back-projection technique for image sequences", *Journal of Computers*, vol. 19, no.3, pp. 44-54. Oct. 2008.
- [23] Yang, Xin-She. Introduction to computational mathematics, *World Scientific*, 2008.
- [24] Yang X. S., "Nature-Inspired Metaheuristic Algorithms", *Luniver Press*, 2008.
- [25] Deb. K., Optimisation for Engineering Design, *Prentice-Hall, New Delhi*, 1995.
- [26] Yang, Xin-She, and Suash Deb. "Cuckoo search via Lévy flights", *NaBIC*, 2009.
- [27] Rajabioun, Ramin. "Cuckoo optimization algorithm." *Applied Soft Computing* vol.11 no.8, pp. 5508-5518, 2011

- [28] Gonzalez, Rafael C., Richard E. Woods, and Steven L. Eddins. "Digital image processing using MATLAB". Vol. 2. Tennessee: Gatesmark Publishing, 2009.
- [29] I. Avcibas,, B. Sankur and K. Sayood, "Statistical evaluation of image quality measures", *Journal of Electronic Imaging*, vol. 11, no.2, pp. 206-223, April 2002.
- [30] M. Cadik and P. Slavik, "Evaluation of two principal approaches to objective image quality assessment," *Eighth International Conference on Information Visualisation, IEEE Computer Society Press*, pp. 513-518, Jul 2004.
- [31] Z. Wang, A. C. Bovik, H. R. Sheikh and E. P. Simoncelli, "Image quality assessment: from error visibility to structural similarity", *IEEE Transactions on Image Processing*, vol. 13, no.4, pp. 600-612, Apr. 2004.